Remote Sensing of Environment 183 (2016) 129–143

Contents lists available at ScienceDirect

Remote Sensing of Environment

journal homepage: www.elsevier.com/locate/rse

Ultra-fine grain landscape-scale quantification of dryland vegetation structure with drone-acquired structure-from-motion photogrammetry

Andrew M. Cunliffe [a,*], Richard E. Brazier [a], Karen Anderson [b]

[a] University of Exeter, Geography, UK
[b] University of Exeter, Environment and Sustainability Institute, UK

ARTICLE INFO

Article history:
Received 21 September 2015
Received in revised form 19 April 2016
Accepted 24 May 2016
Available online xxxx

Keywords:
Semi-arid
Rangeland
Grassland
Shrubland
Vegetation
Biophysical
Biomass
UAV
UAS
SfM
Canopy height model

ABSTRACT

Covering 40% of the terrestrial surface, dryland ecosystems characteristically have distinct vegetation structures that are strongly linked to their function. Existing survey approaches cannot provide sufficiently fine-resolution data at landscape-level extents to quantify this structure appropriately. Using a small, unpiloted aerial system (UAS) to acquire aerial photographs and processing theses using structure-from-motion (SfM) photogrammetry, three-dimensional models were produced describing the vegetation structure of semi-arid ecosystems at seven sites across a grass–to shrub transition zone. This approach yielded ultra-fine (<1 cm^2) spatial resolution canopy height models over landscape-levels (10 ha), which resolved individual grass tussocks just a few cm^3 in volume. Canopy height cumulative distributions for each site illustrated ecologically-significant differences in ecosystem structure. Strong coefficients of determination (r^2 from 0.64 to 0.95) supported prediction of above-ground biomass from canopy volume. Canopy volumes, above-ground biomass and carbon stocks were shown to be sensitive to spatial changes in the structure of vegetation communities. The grain of data produced and sensitivity of this approach is invaluable to capture even subtle differences in the structure (and therefore function) of these heterogeneous ecosystems subject to rapid environmental change. The results demonstrate how products from inexpensive UAS coupled with SfM photogrammetry can produce ultra-fine grain biophysical data products, which have the potential to revolutionise scientific understanding of ecology in ecosystems with either spatially or temporally discontinuous canopy cover.

1. Introduction

Covering 40% of the terrestrial area, dryland ecosystems provide ecosystem services (principally food, but also water and biofuel) that directly support 2.4 billion people (Adeel et al., 2005). These services depend on the vegetation structure of the ecosystems, which is often highly variable through both time and space (Krofcheck et al., 2014; Scott et al., 2016). For example, encroachment of woody shrub vegetation into former grasslands is widely considered to be a mechanism of land degradation (Schlesinger et al., 1990; Adeel et al., 2005; Turnbull et al., 2008), and recent work suggests fluctuations in dryland biomass explain much of the interannual variability and long-term trend in the global terrestrial carbon sink (Poulter et al., 2014; Ahlström et al., 2015). Consequently, knowledge of the changing biophysical structure of dryland vegetation and resulting provision of ecosystem services is necessary for the resilient management of these dynamic landscapes (Adeel et al., 2005; Huang et al., 2009). Such knowledge may also constrain uncertainty surrounding predictions of drylands as major carbon sinks (Poulter et al., 2014; Ahlström et al., 2015; Murray-Tortarolo et al., 2016).

Remote sensing with multispectral imaging has been widely employed to survey vegetation over large extents (e.g. Zhang et al., 2003; White et al., 2009). However, functional inference can be limited by the information content of 2D image data (Krofcheck et al., 2014; Lisein et al., 2013); for example, spectral signatures often have only limited correlation with above-ground biomass (AGB) (Roderick et al., 2000; Friedel et al., 2000; Huang et al., 2007). Monitoring changes and patterns in 3D vegetation structure can be more informative to derive functional understanding (Huenneke et al., 2001; Dandois & Ellis, 2010; Vierling et al., 2013; Calders et al., 2015). AGB is commonly estimated using species-specific, allometric size/biomass regression models, derived using observations from destructive sampling (Huenneke et al., 2001; Allen et al., 2008; Muldavin et al., 2008). On-the-ground monitoring programs employing species-, site-, and year-specific scale-biomass relationships can be accurate, but are labour intensive and susceptible to under-sampling in spatially heterogeneous ecosystems (Huenneke et al., 2001; Rango et al., 2006; Allen et al., 2008; Muldavin et al., 2008; Nafus et al., 2009). Light detection and ranging (LiDAR) is a widely employed surveying technique but has high acquisition costs, limiting the spatial and

* Corresponding author at: University of Exeter, Geography, Amory Building, Rennes Driver, Exeter, Devon, UK.
E-mail addresses: ac365@exeter.ac.uk (A.M. Cunliffe), r.e.brazier@exeter.ac.uk (R.E. Brazier), karen.anderson@exeter.ac.uk (K. Anderson).

http://dx.doi.org/10.1016/j.rse.2016.05.019

temporal scales which can be examined (Vierling et al., 2008; Browning et al., 2015; Calders et al., 2015). These limitations of measurement scale are significant in dryland ecosystems because these systems are often sparsely vegetated with large changes in vegetation structure over relatively short temporal scales, due to wildfires, herbivory or rapid growth following infrequent rainfall events (Friedel et al., 2000; D'Odorico & Porporato, 2006; Huang et al., 2007). This heterogeneity and temporal dynamism contributes to very large, scale-dependent uncertainties associated with estimates of terrestrial carbon stocks (Huenneke et al., 2001; Hill et al., 2013). Constraining these uncertainties requires the development of new techniques to measure terrestrial biomass efficiently and accurately at time-steps that are able to capture the dynamism (Strand et al., 2008; Hill et al., 2013; Murray-Tortarolo et al., 2016).

Anderson and Gaston (2013) suggested that unpiloted aerial systems (UAS) would revolutionise spatial ecology. This paper presents a novel ecological application that validates this assertion, demonstrating the measurement of biomass and carbon stocks in semi-arid ecosystems subject to land degradation. Geoscientists are increasingly utilising fine grain 3D models produced from UAS-acquired image data processed with structure-from-motion (SfM) photogrammetry (e.g. Westoby et al., 2012; Smith & Vericat, 2015; Woodget et al., 2015; Nouwakpo et al., 2015; Tonkin et al., 2014); however, although understanding of SfM photogrammetry is maturing (James & Robson, 2012, 2014; Turner et al., 2014; Smith & Vericat, 2015; Shahbazi et al., 2015), there have been limited applications to use this approach for characterising the biophysical structure of vegetation. Although the potential of UAS-acquired SfM to survey vegetation has been demonstrated for tree-dominated ecosystems (Dandois & Ellis, 2010, 2013; Lisein et al., 2013; Zahawi et al., 2015; Dandois et al., 2015; Puliti et al., 2015), previous work has suggested that SfM modelling of UAS-acquired image data was not yet suitable for measuring the structure of small plants, such as grasses, due to limitations with the accuracy of the derived canopy height models (CHMs) (Zahawi et al., 2015).

Errors in SfM-derived models depend greatly on the quality of geometric control constraining the reconstruction (James & Robson, 2014; Puliti et al., 2015; Shahbazi et al., 2015), and further refinement of the technique was needed to improve measurement accuracy of UAS–SFM approaches to support application to ecosystems dominated by short-sward vegetation (Lisein et al., 2013; Zahawi et al., 2015). Applications of UAS–SfM have generally sought to acquire nadir image data, which is often suggested to reduce distortion (e.g. Dandois & Ellis, 2010, 2013; Dandois et al., 2015; Tonkin et al., 2014; Zahawi et al., 2015). While the acquisition of nadir image data may be necessary for particular applications, such as correcting for refraction in the production of bathymetric maps (Woodget et al., 2015), the inclusion of convergent (non-nadir) image networks has recently been shown to significantly improve the reconstruction accuracy of SfM photogrammetric models (James & Robson, 2014; Smith & Vericat, 2015; Shahbazi et al., 2015).

The objective of this study was to develop a new technique to quantify biomass and associated carbon stocks in heterogeneous and dynamic short sward semi-arid rangelands. UAS-acquired aerial image data were processed with SfM photogrammetry to yield fine-grain 3D models of rangeland ecosystems over landscape extents. Our working hypothesis was that by improving the design of the airborne survey to systematically acquire convergent image data as well as constraining ground control points (GCPs), this technique would be able to characterise vegetation structure in ecosystems dominated by short-sward vegetation and quantify biomass and associated carbon stocks.

2. Methodology

2.1. Study area

The study site was the Sevilleta National Wildlife Refuge in Central New Mexico, USA. Seven areas of interest (AOIs) were surveyed, containing natural vegetation communities. AOIs 1–4, and 7 were situated in the Five Points area of Mackenzie Flats (34.4°N; 106.7°W), a Chihuahuan desert site with a semi-arid climate (mean annual precipitation of 250 mm). This area has experienced long-term encroachment of *Larrea tridentata* (creosotebush shrub) into formerly pristine *Bouteloua eriopoda* and *B. gracilis* (black and blue grama) grasslands (Fig. 1), described further in Turnbull et al. (2010a). AOIs 5 and 6 were located in juniper savanna in the Los Piños Mountain range (34.38°N; 106.52°W), dominated by an overstory of *Juniperus monosperma* (one-seed juniper) with *B. eriopoda* dominated understory and mean annual precipitation of 326 mm (Krofcheck et al., 2014). AOIs 1–6 are described further in Turnbull et al. (2010a); Puttock et al. (2013, 2014) and Cunliffe et al. (2016).

2.2. UAS flights and data acquisition

Fig. 2 presents an overview of the key methodological steps. Image data were acquired under 'leaf-on' conditions in October 2014, using a 3D Robotics Y6 hexacopter equipped with a global navigation satellite system (GNSS) receiver and consumer-grade digital camera (Canon S100), controlled by ArduCopter (V3.2; http://copter.ardupilot.com) software. This platform had a mass of ca. 2.5 kg, and cost less than $3000 USD. All flight operations were conducted within visual line of sight, below a maximum altitude of <120 m above-ground level and within a horizontal distance of <500 m of the operator. Each part of each AOI was surveyed with two fully automatic overflights designed using Open Source Mission Planner (V1.3) software (http://planner.ardupilot.com/). One flight acquired nadir image data and a second acquired convergent (~45° from nadir) image data. The two flights followed perpendicularly-aligned 'lawnmower' survey patterns at 15–20 m altitude, yielding an effective ground sampling distance of 0.004 to 0.007 m per pixel and an effective base-to-height ratio of approximately 0.15.

The inclusion of convergent (non-nadir) image networks is critical to appropriately constrain estimation of both extrinsic (positon and orientation) and intrinsic (lens calibration) parameters estimated during the bundler adjustment step, which significantly influence the reconstruction accuracy of SfM modelling (James & Robson, 2014; Smith & Vericat, 2015; Shahbazi et al., 2015). Convergent image data affords another significant advantage because creosotebush canopies frequently grow in the form of an inverted cone (Singh, 1964; Chew & Chew, 1965; Ludwig et al., 1975; De Soyza et al., 1997; Wainwright et al., 1999; Abrahams et al., 2003), particularly in more arid environments such as the Chihuahuan desert (De Soyza et al., 1997). Consequently, the oblique perspective improves the 'visibility' and thus characterisation of the terrain surface beneath creosotebush canopies, yielding additional ground points, which better constrain the DTM.

The camera was triggered by the autopilot according to distance travelled, attaining 70% forward overlap and 65% sidelap, which combined with the dual flights, meant every part of the AOI was captured in ≥18 photographs. The platform flying speed was varied to ensure a minimum interval between two consecutive images of 2.5 s. Camera shutter speed (Tv) was faster than 1/1250th second, which was sufficient to minimise motion blur at the low flying speeds possible using multi-rotor drones. Camera ISO (Sv) was 200, aperture (Av) was f3.5 and focus was set at infinity. Flights were completed within a few hours of solar midday to minimise shadowing, and sky conditions were generally clear, with some image data acquired during overcast conditions. All seven AOIs were surveyed during 11 days over one month, though it would be straightforward to streamline data acquisition for this combination of spatial extent, spatial resolution and UAV platform to ≤6 days under good weather conditions. Each image was geotagged with the platform's GNSS-derived location, and 10–18 'iron-cross' markers were deployed across each AOI as GCPs and geolocated using differential GNSS [Leica GS08] to a relative spatial accuracy (95% confidence) of 0.015 m in x, y and z (Puttock et al., 2015).

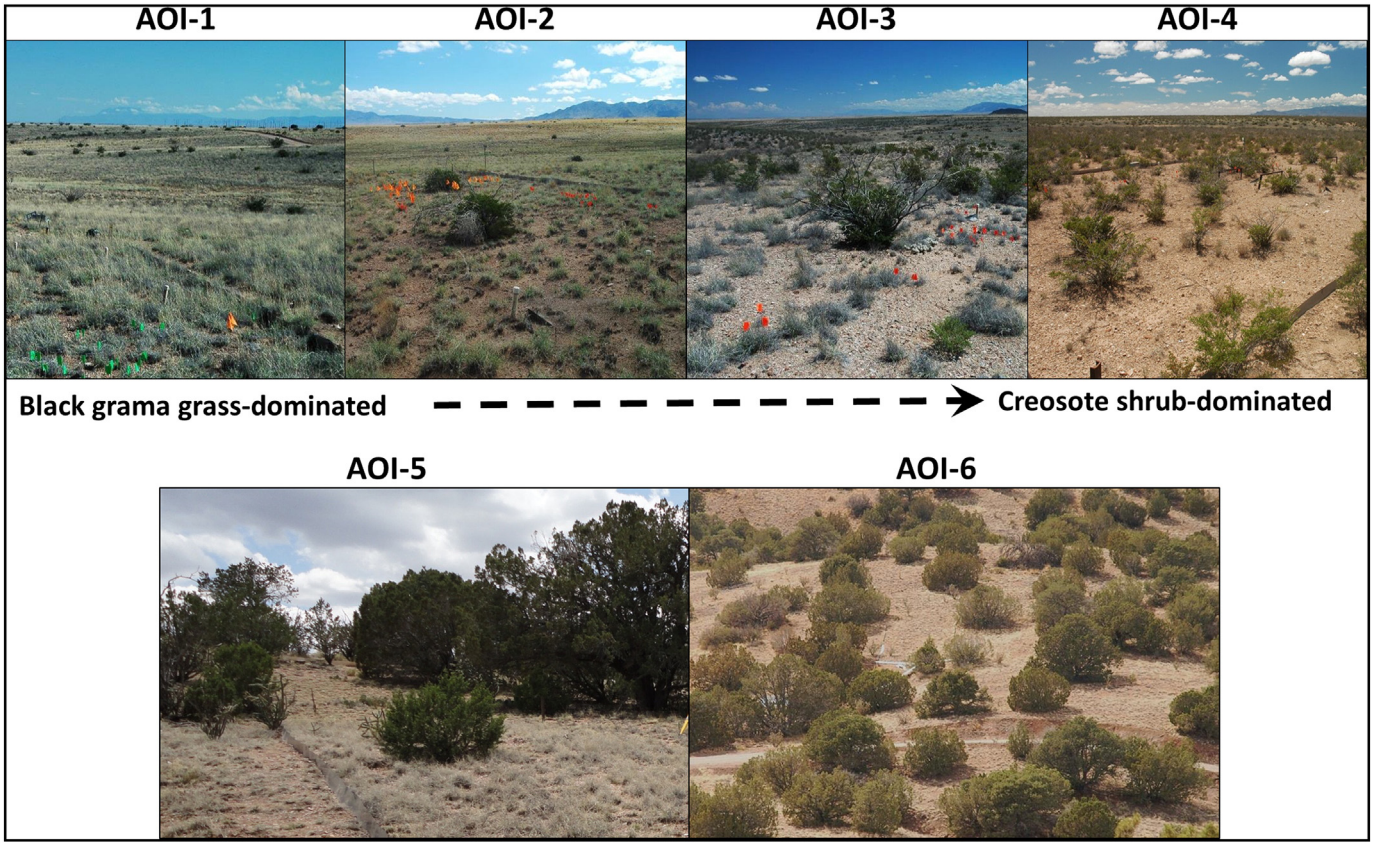

Fig. 1. Photographs of the community assemblages at each AOI, AOI-7 (not shown) is similar to AOI-2. AOIs-1 to -4 illustrate the changed biophysical structure over a grass-shrub ecotone, from black grama-dominated grassland to creosotebush-dominated shrubland. AOI-5 and -6 are juniper savanna. For the colour version of this figure please see the online version of this article.

To assess DTM accuracy, at AOIs 1 to 6, DTM vertical spot height accuracy was assessed against $n = 78–89$ independent DGPS observations (using different locally coordinated benchmarks from the GCP survey).

2.3. SfM photogrammetry processing

SfM and multi-view stereopsis modelling was undertaken on a high performance computer (4 × 16 core AMD Opteron 6276, 512 GB 1600 MHz RAM); although the memory requirements for SfM modelling are high, a lower specification machine can be used if scene areas are modelled in discrete chunks. A range of computer software tools for implementing SfM are available, but for this work Agisoft's PhotoScan (V1.1.0) (http://www.agisoft.com/) was used because it compares favourably with other software in terms of reconstruction detail and accuracy as well as computational efficiency (Dandois & Ellis, 2013; Gini et al., 2013; Turner et al., 2014; Sona et al., 2014; Remondino et al., 2014; Dandois et al., 2015). All processing was undertaken using the highest quality settings, to maximise retention of spatial detail. More than 98.8% of the source image data were aligned and used in the reconstruction for each AOI; alignment of the remaining images was not possible due to insufficient identification of tie points by the image feature descriptor algorithms, and unaligned images were not used in the subsequent modelling.

Direct georeferencing of the image data substantially improves the image alignment process by allowing intelligent comparisons between only nearby images (Agisoft, 2014). This increases computational efficiency, which also enables searching for higher numbers of tie-points and consequently improves the likelihood of successful image alignment (Turner et al., 2014), particularly in texturally complex vegetated scenes (Lisein et al., 2013; Puttock et al., 2015). SfM reconstruction geometric accuracy was optimised through full photogrammetric bundle adjustment, using both direct georeferencing of image data and GCPs in order to refine estimation of the extrinsic and intrinsic parameters of all images. Error terms were specified for both directly georeferenced camera positions (±15 m) and GCPs (±0.015 m). Dense point clouds were produced using multi-view stereopsis to estimate points with both spatial (x, y, z) and spectral (red, green, blue) attributes. Mild-depth filtering was used to reduce erroneous points the dense point cloud while retain points associated with small features of interest such as vegetation elements (Puliti et al., 2015). The seven resultant point clouds each comprised 41–415 million points. Point cloud renderings were produced using the open source software CloudCompare (V2.6.1) (http://www.danielgm.net/cc/).

2.4. DSM, DTM and CHM generation

Digital Surface Model (DSMs) were obtained by applying 10 mm *x,y* grids to the dense point clouds; the highest point in each cell was identified and interpolated linearly (Delaunay triangulation) to a triangular irregular network, which was then sampled regularly at 10 mm spatial resolution. To produce Digital Terrain Models (DTMs) from point clouds it was necessary to identify a subset of points representing ground returns and interpolate between these ground points to produce a continuous surface. The dense point clouds were classified as ground or non-ground, using the two-step classifier implemented in PhotoScan. Firstly, a regular *x,y* grid of a prescribed spatial resolution ('cell size') is applied to the point cloud, the lowest point in each cell is identified and classified as an initial ground point, and these initial ground points are interpolated linearly to produce an approximate initial terrain model. Secondly, all remaining unclassified points are evaluated, and added to the ground class if they meet both of two conditions: (i) They lie below a threshold maximum distance above the initial terrain surface, and (ii) the difference in angle between the closest ground point and the initial terrain surface and the closest initial ground point

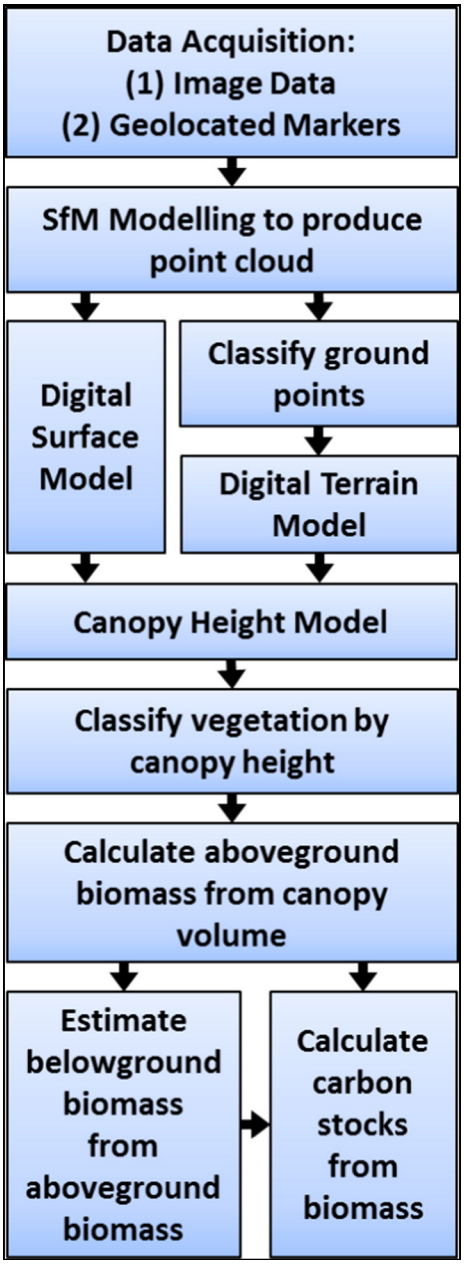

Fig. 2. Workflow outline.

and the point under evaluation is less than a threshold maximum angle (Agisoft, 2014, 2015). This treatment works well for classifying ground points in point clouds with spatially variable density, compromising between accuracy and topographic detail. The cell size parameter is contingent on the minimum density of true ground returns, and must allow every cell to contain at least one ground point.

Maximum distance and maximum angle depend on the degree of topographic variation within each cell; maximum distance represents the maximum permitted maximum variation in Z within any cell and thus is contingent upon the topography and cell size, maximum angle should approximate the maximum gradient of the ground within the AOI. An iterative process was used to identify optimum parameter values to filter non-ground (vegetation) points while maximising retention of topographic detail; these values are optimised for the proportions of the vegetation structure in these ecosystems and are reported in Table 1.

Again 10 mm *x*,*y* grids were applied to the point clouds and in each cell the highest ground point was interpolated (as above); the resultant surface was then regularly sampled at 10 mm spatial resolution. CHMs were derived by subtracting DTMs from DSMs in a GIS (ESRI's ArcMap V10.2.2). Minor errors in DTM and DSM generation resulted in physically impossible negative canopy heights in 0.2% of cells, and negative values were corrected to zero (Dandois & Ellis, 2013). No further smoothing of the CHMs was undertaken.

2.5. Structural classification

The surface cover of each 10 mm cell in the CHM was classified structurally. Modelled canopy heights were used to differentiate bare ground from vegetated cells, with <0.015 m taken to represent bare surfaces, and ≥0.015 m to represent vegetated areas. The accuracy of the bare versus vegetated classification was assessed using visual photo interpretation at 1000 random locations across AOI-7. Vegetated cells were further apportioned between a grass vegetation class and a woody (either shrub or juniper) vegetation class, using a threshold canopy height of 0.2 m to differentiate between grasses (<0.2 m) and woody plants (>0.2 m). While such height-based distinction between plant functional types is a simplification, as the boundary is fuzzy, such approximation is physically reasonable and appropriate in ecosystems where the botanical composition is dominated by differently sized species (Féret & Asner, 2012; Hellesen & Matikainen, 2013). Selection of the 0.2 m threshold was also informed by the natural break in the slope of the canopy height frequency distribution for grass-dominated AOI 1 (depicted in Fig. 7).

2.6. Biomass estimation from CHMs

Commonly measured plant dimensional attributes such as plant height or canopy area are usually non-linearly related to AGB, which necessitates the identification and measurement of individual plants prior to estimation of AGB (e.g. Ludwig et al., 1975; Gholz, 1980; Smith & Brand, 1983; Cleary et al., 2008; Lufafa et al., 2009; Ansley et al., 2012; Mirik et al., 2013). However, for all three vegetation classes considered herein, canopy volume is linearly related to AGB, with an intercept at zero. This linear relationship is fundamental to this approach, as it obviates the need to identify discrete individual plants prior to measuring the volume associated with that class and thus circumvents challenges such as differentiating between neighbouring plants with coalesced canopies, a common occurrence in natural ecosystems (Neufeld et al., 1988; De Soyza et al., 1997). Canopy volume was calculated from CHM, using a foliar canopy approach. For each vegetation class (grass, and shrub or juniper) the volume beneath the ultra-high spatial resolution CHM was summed (Huenneke et al., 2001; Allen et al., 2008; Muldavin et al., 2008; Ladwig et al., 2012).

Foliar canopy approaches to estimating canopy volume are sensitive to subtle differences in plant biophysical structure which do not influence overall plant dimensions (such as maximum height or canopy area); this is particularly important in semi-arid rangeland community assemblages (Neufeld et al., 1988; De Soyza et al., 1997; Rango et al., 2006, 2009). AGB was modelled from canopy volume, using linear regression models developed from published datasets with strong coefficients of determination ($P < 0.001$; $r^2 > 0.64$) and intercepts constrained through the origin, as plants with a canopy volume of zero have no AGB (Muldavin et al., 2008; Ansley et al., 2012). For the grass and shrub classes, volume-AGB data were used from destructive harvesting at the Sevilleta Long Term Ecological Research site between 1999 and 2014 (Moore, 2015). This yielded relationships of AGB [g] = 1053 ± 19.6 × Volume [m^3] ($r^2 = 0.68$, $n = 1383$, ABG between 1 g to 160 g) for *B. eriopoda* and AGB [g] = 1453 ± 72.1 × Volume [m^3] ($r^2 = 0.64$, $n = 228$, ABG between 1 g to 380 g) for *L. tridentata*.

There has been limited whole-tree destructive sampling of juniper and where destructive sampling has been undertaken measured attributes rarely include foliar or canopy volume. To the best of our knowledge, there are no published data on the relationship between canopy

Table 1
AOI descriptions.

Parameter	AOI 1	2	3	4	5	6	7
Vegetation community	Grass-dominated (*Bouteloua eriopoda*)	Grass-Shrub (*B. eriopoda* and *Larrea tridentata*)	Shrub-Grass (*L. tridentata and B. eriopoda*)	Shrub-dominated (*L. tridentata*)	Shrub-Grass (*B. eriopoda*, *Pinus edulis*, and *Juniperus monosperma*)	Grass-Shrub (*B. eriopoda*, *Pinus edulis*, and *Juniperus monosperma*)	Grass-Shrub (*B. eriopoda* and *Larrea tridentata*)
Source Images	135	149	121	253	159	216	2518
% used in reconstruction	99.3	100.0	100.0	100.0	98.7	100.0	98.8
Average GSD [m]	0.004	0.005	0.006	0.004	0.006	0.004	0.007
Coverage [m^2]	4259	4552	7520	4875	10,328	3467	68,222
Parameter sets employed for classification of ground points							
Cell size [m]	0.4	0.4	0.4	0.4	3.0	3.0	0.9
Maximum distance [m]	0.05	0.05	0.05	0.05	0.03	0.03	0.06
Maximum angle [°]	3	3	3	3	1	1	3

volume and AGB for *J. monosperma*. In the absence of species-specific information, volume-biomass regression models were compared for other species of the *Juniperus* genus with similar growth forms. Ansley et al. (2012) reported a relationship of AGB [g] = 23,360 + 2350 × Vol-Volume [m^3] (r^2 = 0.95, n = 40, ABG ranged from 9 kg to 688 kg) for *Juniperus pinchotii* (redberry juniper). Miller et al. (1981) published size and biomass data for *Juniperus osteosperma* (Utah Juniper), the canopies of which commonly exhibit apical dominance; for equivalence with canopy volumes as modelled by UAS–SfM products, canopy volume was calculated as a domed cylinder

$$V = \frac{\left(\frac{\pi a b c}{4}\right)}{2} + \frac{\left(\frac{4}{3}\pi A B \frac{B}{2}\right)}{2} \quad (1)$$

where V = volume [m^3], A = radius of the longest canopy axis [m], B = radius of the perpendicular canopy axis [m], and C = height [m] (adapted from Cleary et al. (2008); Ansley et al. (2012)). This yielded a relationship of AGB [g] = 2149.25 × Volume [m^3] (r^2 = 0.954, $P < 0.000001$, n = 33, AGB between 12 kg to 956 kg) for *J. osteosperma*. The similarity in slopes between the regression models for these two species offers some support for the transfer of the derived relationship between *Juniperus* species with similar growth forms, such as *J. monosperma*, in order to explore the potential of this approach. Reconciling these two models, a coefficient of 2250 was used for the *Juniper* vegetation class.

More powerful predictive models can be developed if volume-biomass relationships are calibrated to the site, year and even phenological stage of dominant plants (Mannetje, 2000; Huenneke et al., 2001; Allen et al., 2008; Muldavin et al., 2008), but the combined relationships are considered to be more transferable spatially and temporally, and were considered appropriate for the present study.

Below-ground biomass (BGB) was inferred from AGB, using root:shoot ratios for each vegetation class derived from meta-analysis

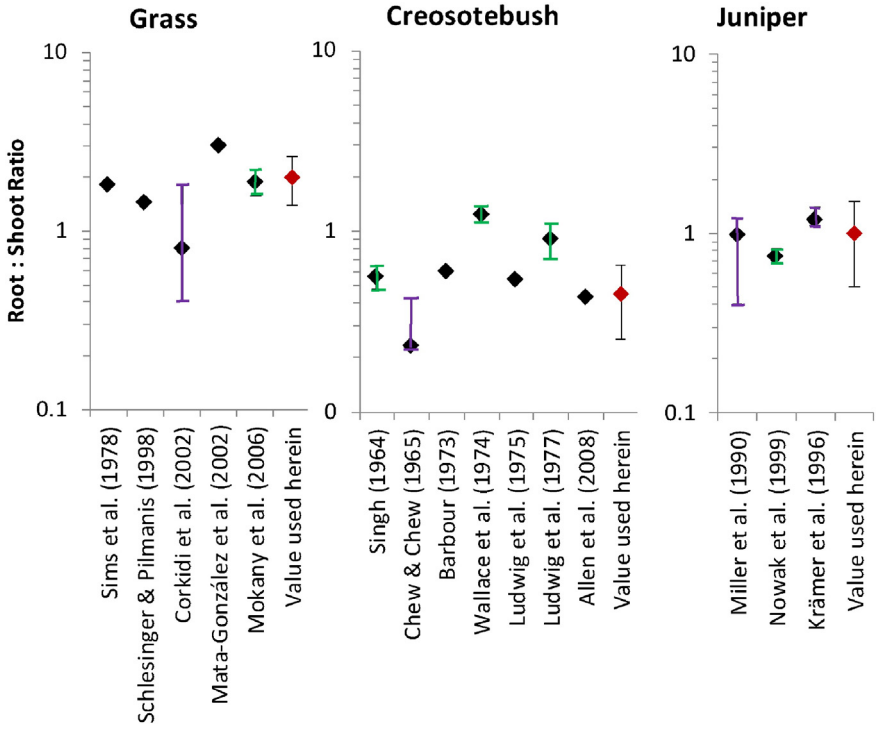

Fig. 3. Meta-analysis of root:shoot ratios reported for black grama (and similar semi-arid) grasses, creosotebush shrubs and juniper trees. Note that logarithmic scales are necessary in (a) to appropriately represent relative differences between root: shoot ratios above and below unity (Cunliffe et al., 2013). Where reported, errors are presented in preference of standard error (Green) > standard deviation (Black) > range (Purple). Values assumed in modelling studies are not plotted. For the colour version of this figure please see the online version of this article.

of published literature, with credence assessed according to sample size, methodological rigour (treatment of leaf matter and fine roots, etc.) and similarity of environmental context to the study site (Fig. 3). Although AGB is a good predictor of BGB for juniper (Krämer et al., 1996; Rozas et al., 2009), again, no published information could be found describing root:shoot ratios for *J. monosperma*; so as above, similar species in the *Juniperus* genus were considered. This yielded root: shoot ratios of 2 ± 0.6 for the semiarid grass class (Sims et al., 1978; Schlesinger & Pilmanis, 1998; Mata-González et al., 2002; Corkidi et al., 2002; Peters, 2002; Mokany et al., 2006), 0.45 ± 0.2 for the creosotebush shrub class (Singh, 1964; Chew & Chew, 1965; Barbour, 1973; Wallace et al., 1974; Ludwig et al., 1975; Ludwig, 1977; Allen et al., 2008), and 1 ± 0.5 for the juniper vegetation class (Miller et al., 1990; Krämer et al., 1996; Nowak et al., 1999; Gentine et al., 2015).

Biomass-carbon conversion coefficients were 0.45 ± 0.03 for grasses (Lieth, 1975; Puttock, 2013), 0.48 ± 0.03 for shrubs (Schlesinger, 1997; Puttock, 2013), and 0.50 ± 0.03 for juniper (Norris et al., 2001; Pregitzer et al., 2002; Strand et al., 2008; Huang et al., 2009; Puttock, 2013). Although biomass-carbon coefficients are likely to differ slightly between AGB and BGB (e.g. Fig. 4), insufficient empirical evidence was available to contain these differences so the same coefficients were applied to both AGB and BGB.

2.7. Treatment of uncertainty

Four main sources of error contribute to the cumulative uncertainty in summary metrics. (i) Minimal empirical information is currently available to constrain error in SfM-derived canopy height models (although see Dandois et al., 2015), but underestimation of canopy volume is more likely so a conservative asymmetric error of −5%/+20% was estimated. (ii) Allometric volume-AGB conversion error was estimated as the 99% confidence interval of the regression error. (iii) Prediction of BGB from AGB is likely to be one of the largest sources of overall uncertainty in total carbon stock estimation because of plasticity in root:shoot ratios in response to soil medium, nutrient and water availability, plant age, and reduction of AGB through herbivory, fire or frost damage (Wallace et al., 1974; Holland et al., 1992; Goodman & Ennos, 1996, 1999; Mokany et al., 2006; Strand et al., 2008; Padilla et al., 2009; Epron et al., 2012; Schlesinger & Bernhardt, 2013a, 2013b). Uncertainty in root:shoot ratios associated with each vegetation class was conservatively estimated, based on variance observed in meta-analysis of published data (Fig. 3). (iv) Errors in the biomass carbon content are usually ignored but can be significant (Lamlom & Savidge, 2003; Thomas & Martin, 2012; Hill et al., 2013), so an estimated error of ±0.03 was specified for all three vegetation classes (Fig. 4). Estimated errors were assumed to be independent and parametrically distributed, and so were propagated using the quadratic approach as the square root of the sum of all squared errors (Taylor, 1997; Asner et al., 2012). Relative to the propagated overall uncertainty, total biomass and total carbon stock estimates were insensitive to differences in the proportion of canopy volume assigned to grass versus shrub/juniper classes. This is important, because it means that these metrics are insensitive to variations in the 0.2 m canopy height threshold used to differentiate grasses from the two woody plant classes.

3. Results

Point-clouds derived using SfM processing of UAS-acquired image data produced photorealistic representations of 3D biotic structure across a range of scales, from grass tussocks 20 mm high to trees several meters high (Fig. 5). All the DSMs and DTMs were free of noticeable doming effects indicative of systematic geometric error in the SfM reconstruction (James & Robson, 2014; Remondino et al., 2014). Comparison between the SfM-derived DTMs and independent DGPS-derived observations of spot heights indicated no meaningful differences (Table 2). The residuals generally have SDs of less than 0.031 m (five of the six AOIs had SD <0.016 m), indicating internal consistency which translates as good relative accuracy. Mean absolute error (MAE)

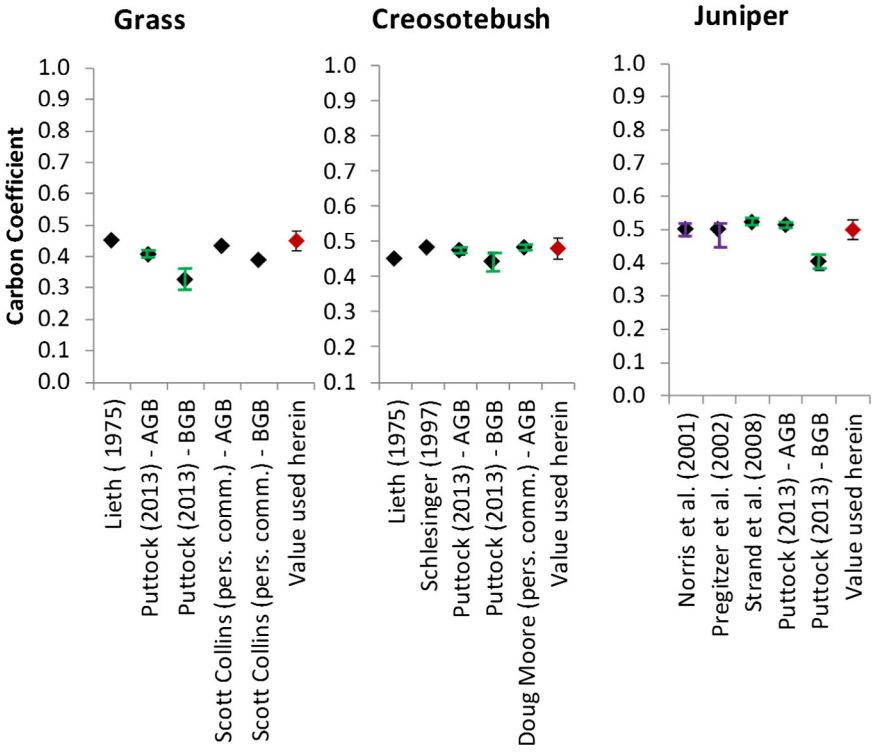

Fig. 4. Meta-analysis of biomass carbon coefficients reported for black grama (and similar semi-arid) grasses, creosotebush shrubs and juniper trees. Where reported, errors are presented in preference of standard error (Green) > standard deviation (Black) > range (Purple). Values assumed in modelling studies are not plotted. For the colour version of this figure please see the online version of this article.

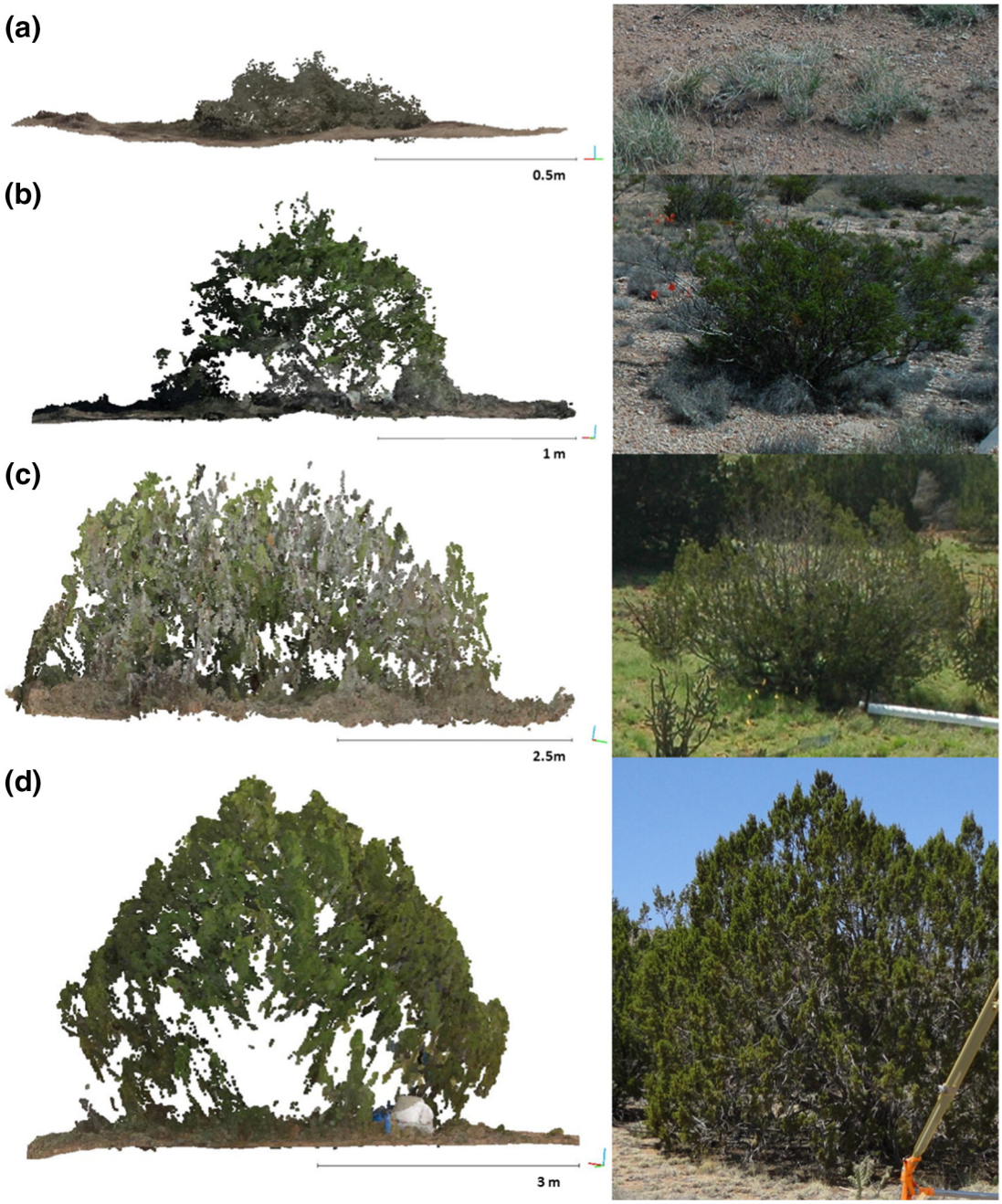

Fig. 5. Renderings of the point clouds representing individual plants: (a) black grama grass (*Bouteloua eriopoda*) (~72,000 points from AOI-2), (b) creosotebush shrub (*Larrea tridentata*) (~250,000 points from AOI-3), (c) and (d) Juniper trees (*Juniperus monosperma*) (~640,000 points and ~713,000 points from AOI-6). Accompanying photographs of each plant individual were taken from slightly different viewpoints to the point cloud renderings. For the colour version of this figure please see the online version of this article.

ranges between −0.077 m and +0.084 m for the six AOIs, this is not significantly greater than the absolute error associated with the benchmarks, indicating no evidence of meaningful error in absolute terms.

Modelled canopy heights were consistent with field observations, and structural classification of surface cover between bare and combined vegetated classes was excellent in comparison with photo-interpretation at 1000 points (overall accuracy >90%, kappa coefficient 0.79) (Table 3). The kappa value of 0.79 implies that the classification

Table 2
DTM accuracy assessment.

Parameter	AOI						
	1	2	3	4	5	6	7
n	83	78	78	79	83	87	NA
Mean absolute error	0.048	0.084	−0.042	−0.016	−0.011	−0.077	NA
(±SD) [m]	0.016	0.015	0.015	0.011	0.014	0.031	NA

Table 3
Error matrix for surface cover classification.

Predictions from canopy height	Reference observations (orthomosaic)			
	Bare	Vegetated	Row total	Commission accuracy
Bare	600	64	664	90.4%
Vegetated	32	304	336	90.5%
Column total	632	368	1000	
Omission accuracy	94.9%	82.6%		
	Overall accuracy:	90.04%	Kappa coefficient:	0.79

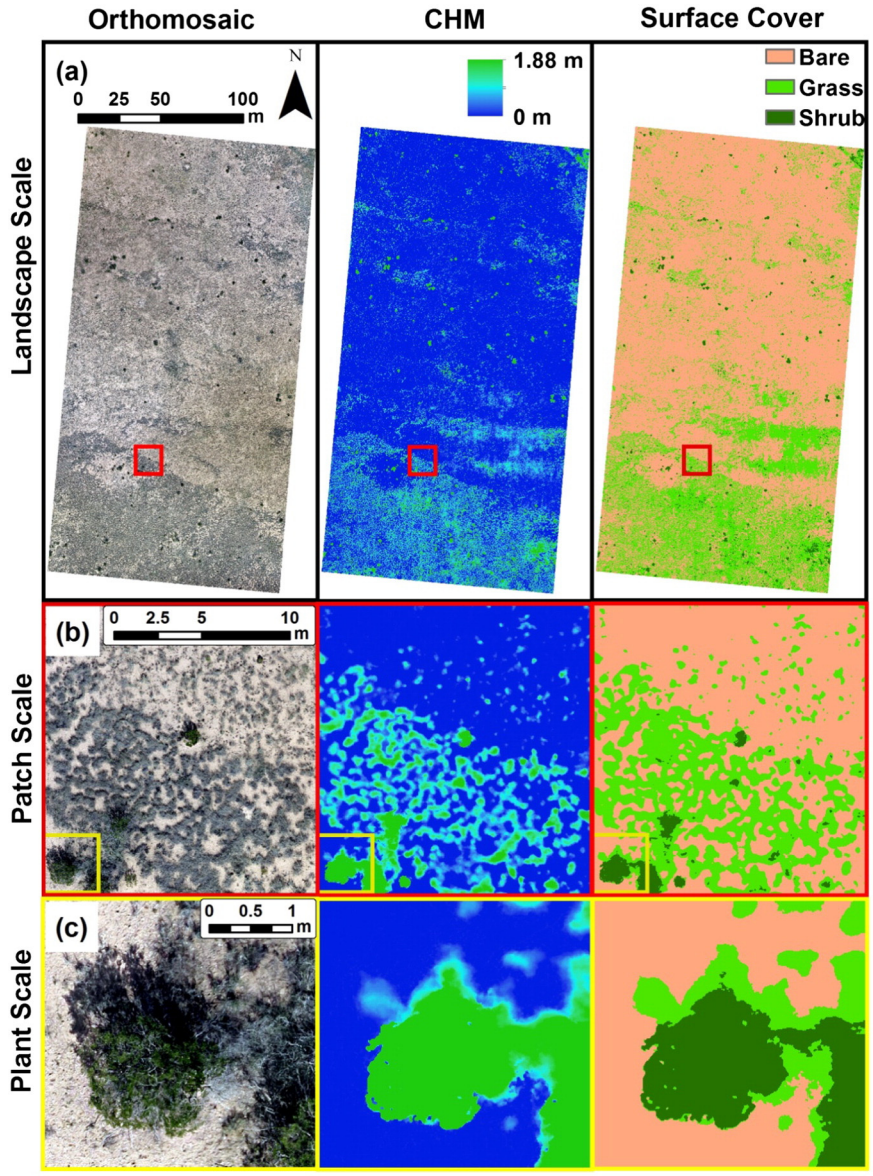

Fig. 6. Three scales of AOI-7 are displayed: landscape (~68,000 m^2), patch (~250 m^2) and plant (~10 m^2). The columns are (i) orthomosaic photograph, (ii) scalar CHM, and (iii) surface cover classified according to modelled canopy height. Magnification increases down through the rows, with the extent each zoom map indicated on the preceding map. For the colour version of this figure please see the online version of this article.

process avoided 79% of the errors that a completely random classification would generate (Congalton, 1991), and can be considered to indicate excellent classifier performance (Landis & Koch, 1977). CHM-inferred classifications of vegetation class (grass versus shrub or juniper) usually agreed with surface cover depicted in the orthomosaic images. An example of the fine grain orthomosaics and digital maps of CHM and surface cover are shown for AOI-7 (Fig. 6). The northern area of AOI-7 was burnt by wildfire on 4th August 2009, five years prior to the present survey (Fig. 6a) and the lasting spatial changes in vegetation pattern can be seen clearly.

The canopy height cumulative distribution functions illustrate several functionally significant differences in ecosystem structure across the ecotone from grass-dominated (AOI-1) to shrub-dominated (AOI-4) vegetation communities (Fig. 7). Across the grass-shrub transition, the proportion of bare surface cover increased from 52% to 89%. The median canopy height of vegetated cells increased from 0.06 m, through 0.07 m, 0.09 m to 0.11 m, for AOI-1–4, respectively. There was a natural break in the canopy heights at ca. 0.2 m in the grass-dominated AOI-1, which

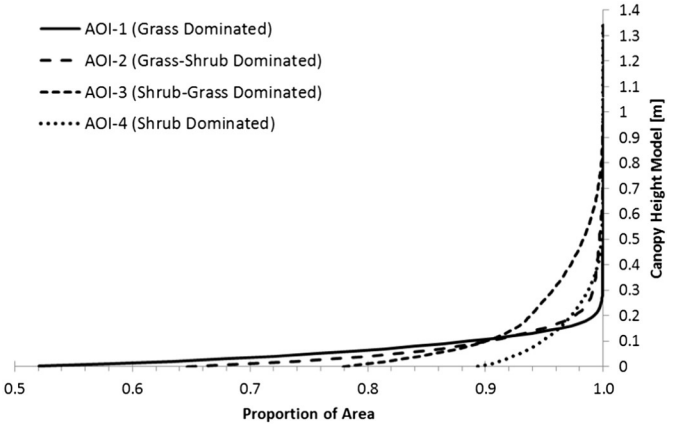

Fig. 7. Canopy height cumulative distribution functions for AOI-1 to AOI-4, across the ecotone from grass-dominated to shrub-dominated vegetation communities.

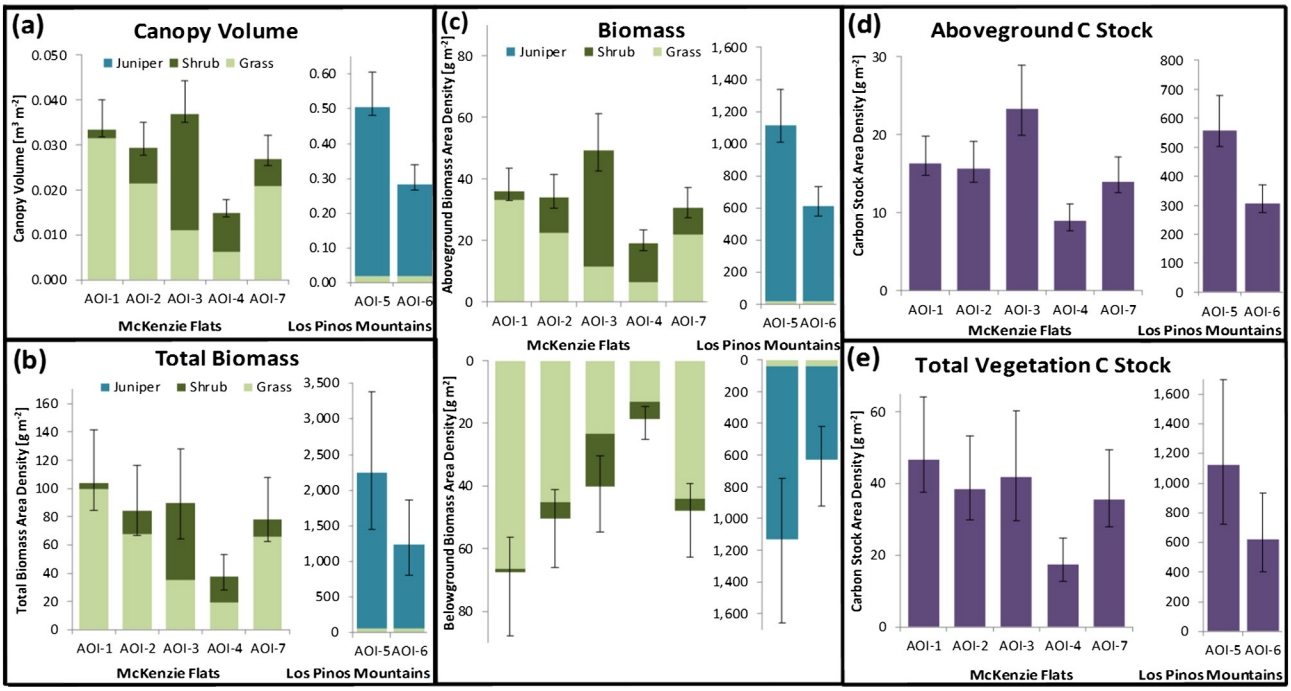

Fig. 8. (a) Measured canopy volumes, (b) total biomass, (c) inferred above-ground biomass (AGB) and below-ground biomass (BGB) for each vegetation class, and estimated (d) above-ground and (e) total vegetation carbon stocks. For the colour version of this figure please see the online version of this article.

corresponds with the typical heights of grass vegetation in these ecosystems. Canopy volume in the juniper-dominated AOIs was an order of magnitude higher than the grass- and shrub-dominated AOIs. Although biomass density did vary between the three vegetation classes, with Juniper (2.25 kg m^3) greater than Creosotebush (1.45 kg m^3) greater than Grass (1.05 kg m^3), trends in AGB across the AOIs reflect those observed in canopy volume (Fig. 8c).

Fig. 8 further exemplifies the information available using this quantitative surveying approach. Across the grass-shrub ecotone grass canopy volume steadily declined; the concomitant increase in shrub volume was less smooth, due to the presence of much larger shrubs in AOI-3 than AOI-4 (Fig. 8a). BGB was dominated by the grass vegetation in the Mackenzie Flats and Juniper vegetation at the Los Piños Mountains, and is subject to higher levels of relative uncertainty due to error in root:shoot ratios. Similar biomass-carbon coefficients between vegetation classes mean that the relative carbon stocks associated with AGB and the total biomass paralleled AGB and total biomass, respectively (Fig. 8d and c).

4. Discussion

4.1. Discussion of methodology

Dandois et al. were the first to demonstrate the capacity of UAS-acquired SfM to characterise vegetation structure at low cost (Dandois & Ellis, 2010, 2013). Work to date has focused on application in forest ecosystems (Dandois & Ellis, 2010, 2013; Lisein et al., 2013; Dandois et al., 2015; Zahawi et al., 2015; Puliti et al., 2015), and indicated that SfM modelling of aerial image data was not yet able to resolve smaller vegetation, such as grasses, due to limitations in the precision of SfM modelling approaches as previously implemented (Zahawi et al., 2015). This study demonstrates that, with appropriate source data, it is possible to constrain SfM modelling in order to overcome this scale limitation.

In order to better constrain SfM modelling and thus reduce error in the resultant information products, this study systematically acquired convergent (non-nadir) image data, in addition to nadir image data and high-precision GCPs (James & Robson, 2014; Smith & Vericat, 2015; Shahbazi et al., 2015). This approach yielded high-precision models, but necessitated multiple overflights of the study areas, doubling field survey effort and also increasing the subsequent computational effort. We hypothesise that there may be an optimum acquisition angle which provides sufficiently convergent image data to adequately constrain SfM modelling, while being sufficiently close to nadir to alleviate the need for additional acquisition of nadir images to ensure sufficient similarity between adjacent images for successful feature matching. Optimal image acquisition angles will be influenced by the nature of the canopy structure; i.e., the perspective required to obtain multiple images of the ground surface through small gaps in high canopies will require near-nadir view angles and high levels of overlap. Furthermore, there are some suggestions that both feature matching and multi-view stereopsis is hindered if view angles exceed 20° (Lowe, 2004; Dandois et al., 2015), although such a limitation is likely to be sensitive to scene structure and complexity. We speculate that an optimum acquisition angle for the biotic structures found in the rangeland ecosystems studied herein may be around 15–25°; although, robustly testing this hypothesis will require a large, multifactorial experiment (e.g. Dandois et al., 2015).

It is constructive to reflect on the use of maximum point elevations within each *x*,*y* cell, as our approach diverges somewhat from the approaches adopted in similar UAS–SfM studies. It is often advocated to use the elevation of a particular percentile within a cell to obtain more representative measurements of canopy height which are less sensitive to possible high outlier points (colloquially described as 'flyers') (Jung et al., 2012; Dandois & Ellis, 2013; Zahawi et al., 2015). These percentile approaches are sensible when characterising large plants at spatial resolutions of >1 m^2, when many points exist within a cell (Dandois & Ellis, 2013; Zahawi et al., 2015). Our use of ultra-fine, cm^2 x,y spatial resolution offers an alternative approach to averaging canopy heights across an AOI, as this similarly restricts the influence of possible outlier points on estimates of overall canopy volume. We suggest that an ultra-fine spatial resolution better utilises the information content in the millions of point observations comprising each point cloud, while affording

greater sensitivity to fine-scale spatio-temporal differences in vegetation biophysical structure which are critically important in grass-shrub ecosystems where plants are low and have a small footprint. Furthermore, our height maxima approach is also consistent with the approaches developed for on-the-ground monitoring of canopy volumes and inferred biomass and associated carbon stocks in these ecosystems (e.g. Huenneke et al., 2001; Allen et al., 2008).

Although the natural colour attributes of SfM-derived point clouds facilitate visual interpretation, this passive remote sensing technology has very limited penetration through vegetation canopies which restricts the number of ground points beneath vegetation canopies (Dandois & Ellis, 2010; Lisein et al., 2013; Dandois et al., 2015). Consequently, UAS-acquired SfM alone may be most usefully applied in ecosystems with spatially or temporally discontinuous vegetation cover, as is common in dryland ecosystems. Alternatively, hybrid approaches have been proposed combining SfM-derived DSMs with DTMs derived from other survey techniques, such as LiDAR (Dandois & Ellis, 2013; Lisein et al., 2013; Dandois et al., 2015; Puliti et al., 2015) or GNSS observations (Zahawi et al., 2015). Such hybrid approaches are promising, although the measurement-scale of CHMs derived using such approaches is limited by the co-registration accuracy of SfM-derived DSMs with the DTMs.

4.2. Biological information content of CHMs

There was good agreement between modelled canopy heights versus our expert knowledge of the vegetation structure derived from many site visits and also subsequent photointerpretation of the ultra-fine spatial resolution orthomosaics. Classification of surface cover between bare and combined vegetated classes on the basis of modelled canopy height exhibited excellent discriminatory accuracy (Overall accuracy 90%, Kappa 0.79) (after Landis & Koch, 1977), indicating that the extent of vegetated cells was well characterised on the basis of modelled canopy heights. Thus our study findings indicate that modelled canopy heights are accurate, at least around the height threshold used to differentiate bare ground from vegetated cells. The <10% errors in the bare versus vegetated classification were predominantly due to incorrect assignment of sparsely vegetated domains to the bare class, overestimating bare cover; this error had little impact on the utility of the bare/vegetated surface cover digital maps. Sparsely vegetated cells are relatively insignificant in terms of several key ecosystem functions, such as their contribution to AGB and grazing potential, modification of raindrop kinetic energy and subsequent particle detachment, or impedance of overland flow (Parsons et al., 1990; Abrahams et al., 1994; Wainwright et al., 1999, 2000). Fires play an important role in many dryland ecosystems (Drewa & Havstad, 2001; Burg et al., 2015). While the enduring effect of historic fire can be faintly observed in the orthophoto through reduced vegetation cover, delineation of the burn extent is much more apparent in the CHM and derived surface cover maps (Fig. 6a). Spatial differences in vegetation structure across the burn boundary differ between the orthomosaic and the CHM-derivatives due to the similarity of spectral signatures between mature and immature vegetation regrowth, in contrast to dissimilarities in biophysical structure (Huang et al., 2007). The spatial differences in vegetation structure are functionally significant, for example in terms of carbon storage and biomass available for livestock forage, and illustrate a key limitation of reliance on 2D image data to monitor biotic structure (Huang et al., 2007). The patch scale (Fig. 6b) depicts the ecological frontier between unburnt and burnt areas. The spatial patterns of surface cover portrayed at these patch scales are major controls on the distribution and erosion-induced redistribution of ecosystem resources in semiarid landscapes, including water, soil and associated chemicals which influence the provision of ecosystem services (Turnbull et al., 2010b; Stewart et al., 2014; Cunliffe et al., 2016).

The plant-scale panels depict a *L. tridentata* individual, illustrating correspondence between the orthomosaic and surface cover classification (Fig. 6c). Fig. 6c exemplifies how CHM-derived classifications are robust against variable illumination (shadowing) which can be problematic for spectral classification approaches (Popescu et al., 2003; Puttock, 2013), particularly in fine resolution image data (Adeline et al., 2013). The 'patchy' shrub canopy shows detail resolved by the ultra-fine spatial resolution which is not resolved in coarser-scale surveys, for example using large-footprint airborne LiDAR. Spatially-distributed, fine grain data describing AGB are invaluable for evaluating numerical models used to test hypotheses regarding complex ecosystem dynamics over a wide variety of spatial and temporal scales (e.g. Stewart et al., 2014; Poulter et al., 2014; Ahlström et al., 2015).

The canopy height distribution functions illustrated in Fig. 7 are biologically more informative than simpler summary metrics such as average canopy height, elucidating functionally-significant differences in community-level ecosystem structure across the ecotone from grass- to shrub-dominated vegetation communities. The spatial patterns observed in canopy height distributions across this grass-shrub are consistent with existing understanding of changes in biophysical structure across this ecotone derived from 2D remote sensing (Turnbull et al., 2010a; Puttock et al., 2013). Critically, because of the spatially contiguous nature of this surveying technique, these cumulative distribution functions summarise upwards of 42 million cells over spatial extents of >4000 m^2, though these extents could easily be increased. Such averaging of large numbers of remotely sensed observations is believed to improve accuracy and sensitivity when measuring community-level traits over large extents (Gobakken & Næsset, 2004; Huang et al., 2009; Puliti et al., 2015). This quantitative approach is sensitive to subtle spatial or temporal differences in biotic structure, yet can rapidly survey relatively large (several ha) spatial extents (Anderson & Gaston, 2013). It can therefore be used to quantify comparatively subtle changes in vegetation structure with small effect sizes, for example in response to herbivory, fire or rainfall, which in turn will support experiments to advance mechanistic understanding of vegetation dynamics at landscape-levels (Friedel et al., 2000). The canopy height cumulative distribution functions illustrate an increase in bare surface cover from 52% to 89%, which is associated with decreased infiltration and increased runoff generation during infrequent but intense rainfall events (Turnbull et al., 2010b; Puttock et al., 2013, 2014).

4.3. Further reflections on UAS–SfM estimation of ecosystem structure

Collecting *appropriate* reference data with which to evaluate UAS SfM-derived CHMs is extremely challenging (Lisein et al., 2013; Dandois et al., 2015; Puliti et al., 2015), and this problem is compounded by difficulties obtaining spatially referenced canopy height observations commensurate with very fine grain CHMs. Previous applications of UAS SfM-derived CHMs have concentrated on silviculture and have typically considered dominant canopy heights for CHM evaluation, using field observations of the average *maximum* height of dominant plants within plots (Dandois & Ellis, 2010, 2013; Lisein et al., 2013; Zahawi et al., 2015; Puliti et al., 2015; Dandois et al., 2015). Metrics of dominant canopy height are however less appropriate in rangeland ecosystems (Lisein et al., 2013), due to the complexity of the shrub canopy architecture and the important contribution of low stature plants to ecosystem AGB (Fig. 8).

Field measurements of grass sward height are multifarious (Mannetje, 2000), but what is measured poorly represents what SfM captures. For example, the highest extremities of grass plants are generally too small and mobile to be represented in UAS SfM- and LiDAR-derived canopy height models, while drop-disk approaches commonly alter sward height through compression as well as covering a much larger extent than the centimetre grain size of the CHMs employed herein (Friedel et al., 2000; Mannetje, 2000). Field measurement of shrub canopies is no less problematic, as shrubs such as creosotebush

are characterised by complex canopy architecture (Wardley et al., 1987; Neufeld et al., 1988; Wilson, 1995; De Soyza et al., 1997) (Figures Figs. 1 and 5). Consequently, foliar volume is frequently a more accurate predictor of AGB than maximum plant height (Neufeld et al., 1988; De Soyza et al., 1997; Huenneke et al., 2001; Rango et al., 2006, 2009; Allen et al., 2008; Muldavin et al., 2008; Ladwig et al., 2012). Plant extremities are often underrepresented in photogrammetric reconstructions (Dandois & Ellis, 2010, 2013; Lisein et al., 2013; Gillan et al., 2014; Zahawi et al., 2015; Dandois et al., 2015), as well as LiDAR surveys (Lefsky et al., 2002; Glenn et al., 2011; Mitchell et al., 2011; Sankey et al., 2013; Li et al., 2015).

Even when the average height is well represented SfM-derived CHMs will often underestimate *maximum* canopy height of individual plants (Dandois et al., 2015). Therefore, we suggest that the *maximum* height of individual plants is not the best metric for evaluating CHM quality, particularly in rangeland ecosystems. To address these important considerations, this study used spatially distributed canopy heights to characterise ecosystem structure, with a conservatively estimated asymmetric error term of $-5\% + 20\%$ for the modelled canopy heights. Critically, these uncertainties do not mask the main vegetation patterns, and do not prohibit meaningful estimates of biomass in these ecosystems. More work is needed to refine validation of this approach in rangeland environmental contexts, which should include more destructive sampling of individual plants whose canopy volume has first been measured using UAS SfM under field conditions. It is also pertinent to exercise caution when evaluating estimates of AGB obtained from UAS SfM CHMs against estimates of AGB derived from other forms of allometry (e.g. AGB estimated from breast height diameter), as both forms of allometry have uncertainties which should be explicitly considered (Puliti et al., 2015).

Critically for biomass estimation, in this study foliar volume was linearly related to AGB and had an intercept of zero for all three plant functional types. Consequently, in this study it was not necessary to employ object-based classification approaches to isolate individual plants, in contrast to when measured plant attributes are non-linearly related to AGB (e.g. Ludwig et al., 1975; Gholz, 1980; Smith & Brand, 1983; Northup et al., 2005; Cleary et al., 2008; Lufafa et al., 2009; Ansley et al., 2012; Mirik et al., 2013; Sankey et al., 2013). Avoiding the requirement of identifying individual plants is valuable in structurally complex natural ecosystems where the canopies of neighbouring plants commonly coalesce, confounding distinction between individuals (e.g. Ffolliott & Gottfried, 2002; Strand et al., 2008). Furthermore, this approach can be applied across a very wide range of plant sizes (spanning three orders of magnitude), alleviating the need to exclude biomass associated with smaller plants from carbon accounting (Strand et al., 2008; Asner et al., 2012; Sankey et al., 2013).

Our estimates of AGB in ecosystems dominated by the three species considered herein are consistent with the magnitudes of biomass stocks reported for similar ecosystems (e.g. Barbour et al., 1977; Sankey et al., 2013). Note that the biomass density is likely to vary to some extent with phenological state (Huenneke et al., 2001; Yao et al., 2006; Allen et al., 2008; Muldavin et al., 2008); consequently, care should be taken to evaluate the temporal stability of the relationship between canopy volume and AGB if this approach is employed to characterise AGB of an ecosystem during different phenological states.

4.4. Future applications of UAS–SfM in rangelands

UAS-acquired SfM has substantial potential to revolutionise the study of ecosystem dynamics (sensu Anderson & Gaston, 2013). Because ultra-fine grain CHMs have not previously been widely available there has been limited research on their validation or utilisation. Herein, we answer the call for new techniques to measure above-ground biomass (Hill et al., 2013) and demonstrate how an emerging technology can fulfil the need for scale-appropriate (fine-resolution and large spatial extent) measurements. Such quantitative descriptions of plant architecture at centimetre scales are essential to elucidate the dynamics of ecosystems subject to significant environmental change (Getzin et al., 2014; Stewart et al., 2014; Poulter et al., 2014; Ahlström et al., 2015). Foliar volume measurements from UAS-acquired SfM are of comparable measurement-scale to data obtained from on-the-ground surveying (Huenneke et al., 2001; Yao et al., 2006; Allen et al., 2008; Muldavin et al., 2008), facilitating both validation and integration of ecosystem knowledge derived from these two complementary approaches. Although direct estimation of AGB on the basis of foliar volume is a well-established technique in on-the-ground monitoring of rangeland vegetation dynamics (Huenneke et al., 2001; Herrick et al., 2005; Allen et al., 2008), foliar volume measured using remote sensed fine grain CHMs has not been widely used to directly predict AGB. Because high-precision, fine grain CHMs directly account for some variation in growth form between plant individuals, we believe these approaches are likely to be more accurate and sensitive predictors of AGB than simpler metrics such as maximum plant height or canopy area.

Fine-grain CHMs could be applied to advance understanding of vegetation self-organization in 3D, progressing beyond the insights supported by 2D approaches. For example, although most plant species exhibit no orientation relative to azimuth (Kimes, 1984; Falster and Westoby, 2003; McNeil et al., 2016), creosotebush branches and canopies are often orientated to face the southeast (Neufeld et al., 1988; Whitford et al., 1995). Creosotebush orientation is hypothesised to optimise water use efficiency by maximising interception of insolation earlier in the day when air temperatures are lower, as air temperatures rise during each day, stomatal closure to reduce transpiration losses limits gas exchange and thus photosynthesis (Neufeld et al., 1988; Whitford et al., 1995). UAS–SfM could be used to efficiently characterise creosotebush canopies, for example across the climatic range of this species, and could further elucidate the controls on orientation in vegetation canopies.

UAS-acquired SfM approaches can be used to survey extents diametrically equivalent to coarse-grain, satellite-derived, globally-available products describing vegetation structure, at least at the scale of several ha (Dandois & Ellis, 2013; Browning et al., 2015). Therefore, fine grain, spatially distributed datasets quantifying spatiotemporal variations in AGB could be used to facilitate scaling studies to understand the accuracy and sensitivity of globally-available information products used for biomass estimation in drylands globally, such as the Moderate Resolution Imaging Spectroradiometer (MODIS) (Zhang & Kondragunta, 2006; Muukkonen & Heiskanen, 2007; Baccini et al., 2008) or vegetation optical depth (VOD) (Owe et al., 2001; Liu et al., 2013a, 2013b; Murray-Tortarolo et al., 2016). For example, MODIS pixels cover an area ~20,000 times greater than that observed by cameras typically installed on eddy covariance flux towers, hindering comparisons of vegetation phenology observed at these measurement scales (Balzarolo et al., 2016). Hierarchal modelling approaches (e.g. Wilson et al., 2011) are particularly promising for such upscaling efforts. High quality datasets describing spatial and temporal changes in AGB are also needed to critically evaluate the performance of dynamic vegetation models (Chave et al., 2004), particularly in dryland regions (Poulter et al., 2014; Ahlström et al., 2015). Such dynamic vegetation models are an important component of the Earth System Models used to simulate global scale phenomenon and investigate possible future states of the Earth System, and improving the empirical foundation of these models is essential to improve understanding of the role of dryland ecosystems in both long term trends and interannual variability in the global land carbon sink (Poulter et al., 2014; Ahlström et al., 2015). High-quality datasets describing temporal vegetation dynamics in grass and shrub dominated rangeland ecosystems are particularly required, because recent studies have highlighted significant disagreements between current dynamic vegetation model predictions and the limited empirical observations, indicating the need for further model refinement (Murray-Tortarolo et al., 2016).

5. Conclusion

This study demonstrated how ecosystem biotic structure can be efficiently characterised at cm scales using SfM photogrammetry to process aerial photographs captured from a lightweight UAS costing less than $3000 USD. The well-constrained SfM reconstructions resolved individual plants just a few cm^3 in volume over areas of 10 ha, a level of detail hitherto unobtainable using the UAS-acquired SfM approach. Canopy volumes derived from the CHMs can be used to infer above-ground biomass, and subsequently belowground biomass and associated carbon stocks. Using this UAS-acquired SfM approach, ultra-fine grain CHMs can be obtained at much lower cost than comparable LiDAR datasets. The measurements are sensitive to subtle spatio-temporal changes in biophysical structure, as demonstrated by the survey over the recently burned area and could easily be acquired at daily timesteps over extents of ~1–5 ha. Compared to on-the-ground surveys, this coverage yields more spatially-representative assessments of ecosystem state, facilitating the extraction of subtle signals that elucidate significant controls on biophysical and ecohydrological processes. The technique has the potential to revolutionise monitoring of biophysical structure over landscape-levels in ecosystems with spatio-temporally discontinuous canopy covers. Such data could reduce uncertainty in biomass inventories, and allow previously unfeasible experiments on process interactions in a range of environmental contexts. For example, the capacity to survey areas diametrically equivalent to coarse-grain information products such as MODIS at spatial resolutions comparable to on-the-ground monitoring would facilitate upscaling studies, the impact of different intensities of herbivory on AGB under various environmental conditions could be quantified, and vegetation responses to precipitation inputs in water-limited ecosystems could be characterised at landscape-levels on very short timesteps. The inexpensive approach presented herein is highly complementary to existing approaches for monitoring biophysical structure, and represents an appreciable advance in the tools available to ecologists.

Acknowledgements

This research was supported by a NERC PhD studentship (NE/K500902/1) and Sevilleta LTER program research fellowship (NSF grant DEB-1232294) both awarded to AMC; neither funder had any further involvement in this experiment and the authors declare no conflict of interest. We thank Scott Collins, the Sevilleta LETR director and US Fish and Wildlife for their support during this research and for granting access to the field site. The 3D Robotics Y6 was supplied by the University of Exeter Environment and Sustainability Institute's (ESI) Environmental Monitoring DroneLab (EMDL). The authors wish to express their thanks to Leon DeBell and Agisoft's Alexey Pasumansky for the excellent technical support, to Susan Beck and Phil Cunliffe for facilitating access to archival material, and to Isla Myers-Smith and three anonymous reviewers whose comments allowed us to improve an earlier draft of this article. For access to the data presented herein please contact the first author.

References

Abrahams, A. D., Parsons, A. J., & Wainwright, J. (1994). Resistance to overland flow on semiarid grassland and shrubland hillslopes, Walnut Gulch, southern Arizona. *Journal of Hydrology*, *156*, 431–446.

Abrahams, A. D., Parsons, A. J., & Wainwright, J. (2003). Disposition of rainwater under creosotebush. *Hydrological Processes*, *17*, 2555–2566. http://dx.doi.org/10.1002/hyp.1272.

Adeel, Z., Safriel, U., Niemeijer, D., & White, R. (2005). *Ecosystems and human wellbeing: Desertification synthesis. Millennium Ecosystem Assessment*. Washington, D.C.: World Resources Institute.

Adeline, K. R. M., Chen, M., Briottet, X., Pang, S. K., & Paparoditis, N. (2013). Shadow detection in very high spatial resolution aerial images: A comparative study. *ISPRS Journal of Photogrammetry and Remote Sensing*, *80*, 21–38. http://dx.doi.org/10.1016/j.isprsjprs.2013.02.003.

Agisoft (2014). *Agisoft PhotoScan user manual: Professional edition, V 1.1.0, Agisoft.*

Agisoft (2015). *Agisoft PhotoScan user manual: Professional edition, V 1.2.0, Agisoft.*

Ahlström, A., et al. (2015). The dominant role of semi-arid ecosystems in the trend and variability of the land CO_2 sink. *Science*, *348*(6237), 895–899. http://dx.doi.org/10.1126/science.aaa1668.

Allen, A. P., Pockman, W. T., Restrepo, C., & Milne, B. T. (2008). Allometry, growth and population regulation of the desert shrub *Larrea tridentata*. *Functional Ecology*, *22*(2), 197–204. http://dx.doi.org/10.1111/j.1365-2435.2007.01376.x.

Anderson, K., & Gaston, K. J. (2013). Lightweight unmanned aerial vehicles (UAVs) will revolutionise spatial ecology. *Frontiers in Ecology and the Environment*, *11*(3), 138–146. http://dx.doi.org/10.1890/120150.

Ansley, R. J., Mirik, M., Surber, B. W., & Park, S. C. (2012). Canopy area and aboveground mass of individual redberry juniper (*Juniperus pinchotii*) trees. *Rangeland Ecology & Management*, *65*(2), 189–195. http://dx.doi.org/10.2111/REM-D-11-00112.1.

Asner, G. P., et al. (2012). High-resolution mapping of forest carbon stocks in the Colombian Amazon. *Biogeosciences*, *9*(7), 2683–2696. http://dx.doi.org/10.5194/bg-9-2683-2012.

Baccini, A., Laporte, N., Goetz, S. J., Sun, M., & Dong, H. (2008). A first map of tropical Africa's above-ground biomass derived from satellite imagery. *Environmental Research Letters*, *3*(4), 045011. http://dx.doi.org/10.1088/1748-9326/3/4/045011.

Balzarolo, M., et al. (2016). Matching the phenology of net ecosystem exchange and vegetation indices estimated with MODIS and FLUXNET in-situ observations. *Remote Sensing of Environment*, *174*, 290–300. http://dx.doi.org/10.1016/j.rse.2015.12.017.

Barbour, M. G. (1973). Desert dogma reexamined: Root/shoot productivity and plant spacing. *American Midland Naturalist*, *89*(1), 41–57. http://dx.doi.org/10.2307/2424134.

Barbour, M. G., MacMahon, J. A., Bamberg, S. A., & Ludwig, J. A. (1977). The structure and distribution of *Larrea* communities. In T. H. Mabry, J. H. Hunziker, & D. R. Difeo (Eds.), *Creosote bush: Biology and chemistry of Larrea in new world deserts* (pp. 227–251). Stroudverg: Dowden, Hutchinson and Ross.

Browning, D. M., Rango, A., Karl, J. W., Laney, C. M., Vivoni, E. R., & Tweedie, C. E. (2015). Emerging technological and cultural shifts advancing drylands research and management. *Frontiers in Ecology and the Environment*, *13*(1), 52–60. http://dx.doi.org/10.1890/140161.

Burg, D., Malkinson, D., Katriel, G., & Wittenberg, L. (2015). Modeling the dynamics of soil erosion and vegetative control — Catastrophe and hysteresis. *Theoretical Ecology*, *8*(1), 67–79. http://dx.doi.org/10.1007/s12080-014-0233-9.

Calders, K., et al. (2015). Nondestructive estimates of above-ground biomass using terrestrial laser scanning. *Methods in Ecology and Evolution*, *6*(2), 198–208. http://dx.doi.org/10.1111/2041-210X.12301.

Chave, J., Condit, R., Aguilar, S., Hernandez, A., Lao, S., & Perez, R. (2004). Error propagation and scaling for tropical forest biomass estimates. *Philosophical Transactions of the Royal Society of London B: Biological Sciences*, *359*(1443), 409–420. http://dx.doi.org/10.1098/rstb.2003.1425.

Chew, R. M., & Chew, A. E. (1965). The primary productivity of a desert-shrub (*Larrea tridentata*) community. *Ecological Monographs*, *35*(4), 355–375. http://dx.doi.org/10.2307/1942146.

Cleary, M. B., Pendall, E., & Ewers, B. E. (2008). Testing sagebrush allometric relationships across three fire chronosequences in Wyoming, USA. *Journal of Arid Environments*, *72*(4), 285–301. http://dx.doi.org/10.1016/j.jaridenv.2007.07.013.

Congalton, R. G. (1991). A review of assessing the accuracy of classifications of remotely sensed data. *Remote Sensing of Environment*, *37*(1), 35–46. http://dx.doi.org/10.1016/0034-4257(91)90048-B.

Corkidi, L., Rowland, D. L., Johnson, N. C., & Allen, E. B. (2002). Nitrogen fertilization alters the functioning of arbuscular mycorrhizas at two semiarid grasslands. *Plant and Soil*, *240*(2), 299–310. http://dx.doi.org/10.1023/A:1015792204633.

Cunliffe, A. M., Baird, A. J., & Holden, J. (2013). Hydrological hotspots in blanket peatlands: Spatial variation in peat permeability around a natural soil pipe. *Water Resources Research*, *49*(9), 5342–5354. http://dx.doi.org/10.1002/wrcr.20435.

Cunliffe, A. M., Puttock, A. K., Turnbull, L., Wainwright, J., & Brazier, R. E. (2016). Dryland, calcareous soils store (and lose) significant quantities of near-surface organic carbon. *Journal of Geophysical Research, Earth Surface*. http://dx.doi.org/10.1002/2015JF003628.

D'Odorico, P., & Porporato, A. (2006). Soil moisture dynamics in water-limited ecosystems. In P. D'Odorico, & A. Porporato (Eds.), *Dryland Ecohydrology* (pp. 31–46). Springer.

Dandois, J. P., & Ellis, E. C. (2010). Remote sensing of vegetation structure using computer vision. *Remote Sensing*, *2*(4), 1157–1176. http://dx.doi.org/10.3390/rs2041157.

Dandois, J. P., & Ellis, E. C. (2013). High spatial resolution three-dimensional mapping of vegetation spectral dynamics using computer vision. *Remote Sensing of Environment*, *136*, 259–276. http://dx.doi.org/10.1016/j.rse.2013.04.005.

Dandois, J. P., Olano, M., & Ellis, E. C. (2015). Optimal altitude, overlap, and weather conditions for computer vision UAV estimates of forest structure. *Remote Sensing*, *7*(10), 13895–13920. http://dx.doi.org/10.3390/rs71013895.

De Soyza, A. G., Whitford, W. G., Martinez-Meza, E., & Van Zee, J. W. (1997). Variation in creosotebush (*Larrea tridentata*) canopy morphology in relation to habitat, soil fertility and associated annual plant communities. *American Midland Naturalist*, *137*(1), 13–26. http://dx.doi.org/10.2307/2426751.

Drewa, P. B., & Havstad, K. M. (2001). Effects of fire, grazing, and the presence of shrubs on Chihuahuan desert grasslands. *Journal of Arid Environments*, *48*, 429–443. http://dx.doi.org/10.1006/jare.2000.0769.

Epron, D., Nouvellon, Y., & Ryan, M. G. (2012). Introduction to the invited issue on carbon allocation of trees and forests. *Tree Physiology*, *32*(6), 639–643. http://dx.doi.org/10.1093/treephys/tps055.

Falster, D. S., & Westoby, M. (2003). Leaf size and angle vary widely across species: What consequences for light interception? *New Phytologist*, *158*(3), 509–525. http://dx.doi.org/10.1046/j.1469-8137.2003.00765.x.

Féret, J. -B., & Asner, G. P. (2012). Semi-supervised methods to identify individual crowns of lowland tropical canopy species using imaging spectroscopy and LiDAR. *Remote Sensing*, *4*(8), 2457–2476. http://dx.doi.org/10.3390/rs4082457.

Ffolliott, P. F., & Gottfried, G. J. (2002). *Dynamics of a Pinyon-Juniper stand in Northern Arizona: A half-century history. Research Paper*. CO, USA: Department of Agriculture, Forest Service, Rocky Mountain Research Station, Fort Collins.

Friedel, M. H., Laycock, W. A., & Bastin, G. N. (2000). Assessing rangeland condition and trend. In L.'t. Mannetje, & R. M. Jones (Eds.), *Field and laboratory methods for grassland and animal production research* (pp. 227–262). New York, NY, USA: CABI Publishing.

Gentine, P., Guérin, M., Uriarte, M., McDowell, N. G., & Pockman, W. T. (2015). An allometry-based model of the survival strategies of hydraulic failure and carbon starvation. *Ecohydrology*. http://dx.doi.org/10.1002/eco.1654 (n/a–n/a).

Getzin, S., Nuske, R. S., & Wiegand, K. (2014). Using unmanned aerial vehicles (UAV) to quantify spatial gap patterns in forests. *Remote Sensing*, *6*(8), 6988–7004. http://dx.doi.org/10.3390/rs6086988.

Gholz, H. L. (1980). Structure and productivity of *Juniperus occidentalis* in central oregon. *American Midland Naturalist*, *103*(2), 251–261. http://dx.doi.org/10.2307/2424623.

Gillan, J. K., Karl, J. W., Duniway, M., & Elaksher, A. (2014). Modeling vegetation heights from high resolution stereo aerial photography: An application for broad-scale rangeland monitoring. *Journal of Environmental Management*, *144*, 226–235. http://dx.doi.org/10.1016/j.jenvman.2014.05.028.

Gini, R., Pagliari, D., Passoni, D., Pinto, L., Sona, G., & Dosso, P. (2013). UAV photogrammetry: Block triangulation comparisons, *ISPRS - International Archives of the Photogrammetry. Remote Sensing and Spatial Information Sciences*, *XL-1*(W2), 157–162. http://dx.doi.org/10.5194/isprsarchives-XL-1-W2-157-2013.

Glenn, N. F., Spaete, L. P., Sankey, T. T., Derryberry, D. R., Hardegree, S. P., & Mitchell, J. J. (2011). Errors in LiDAR-derived shrub height and crown area on sloped terrain. *Journal of Arid Environments*, *75*(4), 377–382. http://dx.doi.org/10.1016/j.jaridenv.2010.11.005.

Gobakken, T., & Næsset, E. (2004). Estimation of diameter and basal area distributions in coniferous forest by means of airborne laser scanner data. *Scandinavian Journal of Forest Research*, *19*(6), 529–542. http://dx.doi.org/10.1080/02827580410019454.

Goodman, A. M., & Ennos, A. R. (1996). A comparative study of the response of the roots and shoots of sunflower and maize to mechanical stimulation. *Journal of Experimental Botany*, *47*(10), 1499–1507. http://dx.doi.org/10.1093/jxb/47.10.1499.

Goodman, A. M., & Ennos, A. R. (1999). The effects of soil bulk density on the morphology and anchorage mechanics of the root systems of sunflower and maize. *Annals of Botany*, *83*(3), 293–302. http://dx.doi.org/10.1006/anbo.1998.0822.

Hellesen, T., & Matikainen, L. (2013). An object-based approach for mapping shrub and tree cover on grassland habitats by use of LiDAR and CIR orthoimages. *Remote Sensing*, *5*(2), 558–583. http://dx.doi.org/10.3390/rs5020558.

Herrick, J. E., Van Zee, J. W., Havstad, K. M., Burkett, L., & Whitford, W. G. (2005). *Monitoring manual for grassland, shrubland and savanna ecosystems. Volume I: Quick Start and Volume II: Design. Supplementary Methods and Interpretation., USDA-ARS Jornada Experimental Range, Las Cruces, NM, UAS.*

Hill, T. C., Williams, M., Bloom, A. A., Mitchard, E. T. A., & Ryan, C. M. (2013). Are inventory based and remotely sensed above-ground biomass estimates consistent? *PloS One*, *8*(9), e74170. http://dx.doi.org/10.1371/journal.pone.0074170.

Holland, E. A., Parton, W. J., Detling, J. K., & Coppock, D. L. (1992). Physiological responses of plant populations to herbivory and their consequences for ecosystem nutrient flow. *The American Naturalist*, *140*(4), 685–706.

Huang, C., Asner, G. P., Martin, R. E., Barger, N. N., & Neff, J. C. (2009). Multiscale analysis of tree cover and aboveground carbon stocks in pinyon–juniper woodlands. *Ecological Applications*, *19*(3), 668–681. http://dx.doi.org/10.1890/07-2103.1.

Huang, C. -Y., Marsh, S. E., McClaran, M. P., & Archer, S. R. (2007). Postfire stand structure in a semiarid savanna: Cross-scale challenges estimating biomass. *Ecological Applications*, *17*(7), 1899–1910. http://dx.doi.org/10.1890/06-1968.1.

Huenneke, L. F., Clason, D., & Muldavin, E. (2001). Spatial heterogeneity in Chihuahuan Desert vegetation: Implications for sampling methods in semi-arid ecosystems. *Journal of Arid Environments*, *47*, 257–270. http://dx.doi.org/10.1006/jare.2000.0678.

James, M. R., & Robson, S. (2012). Straightforward reconstruction of 3D surfaces and topography with a camera: Accuracy and geoscience application. *Journal of Geophysical Research*, *117*, F03017. http://dx.doi.org/10.1029/2011JF002289.

James, M. R., & Robson, S. (2014). Mitigating systematic error in topographic models derived from UAV and ground-based image networks. *Earth Surface Processes and Landforms*, *39*(10), 1413–1420. http://dx.doi.org/10.1002/esp.3609.

Jung, K., Kaiser, S., Böhm, S., Nieschulze, J., & Kalko, E. K. V. (2012). Moving in three dimensions: Effects of structural complexity on occurrence and activity of insectivorous bats in managed forest stands. *Journal of Applied Ecology*, *49*(2), 523–531. http://dx.doi.org/10.1111/j.1365-2664.2012.02116.x.

Kimes, D. S. (1984). Modeling the directional reflectance from complete homogeneous vegetation canopies with various leaf-orientation distributions. *Journal of the Optical Society of America. A*, *1*(7), 725–737. http://dx.doi.org/10.1364/JOSAA.1.000725.

Krämer, S., Miller, P. M., & Eddleman, L. E. (1996). Root system morphology and development of seedling and juvenile *Juniperus occidentalis*. *Forest Ecology and Management*, *86*(1–3), 229–240. http://dx.doi.org/10.1016/S0378-1127(96)03769-3.

Krofcheck, D. J., Eitel, J. U. H., Vierling, L. A., Schulthess, U., Hilton, T. M., Dettweiler-Robinson, E., ... Litvak, M. E. (2014). Detecting mortality induced structural and functional changes in a piñon–juniper woodland using Landsat and RapidEye time series. *Remote Sensing of Environment*, *151*, 102–113. http://dx.doi.org/10.1016/j.rse.2013.11.009.

Ladwig, L. M., Collins, S. L., Swann, A. L., Xia, Y., Allen, M. F., & Allen, E. B. (2012). Above- and belowground responses to nitrogen addition in a Chihuahuan Desert grassland. *Oecologia*, *169*(1), 177–185. http://dx.doi.org/10.1007/s00442-011-2173-z.

Lamlom, S. H., & Savidge, R. A. (2003). A reassessment of carbon content in wood: Variation within and between 41 North American species. *Biomass and Bioenergy*, *25*(4), 381–388. http://dx.doi.org/10.1016/S0961-9534(03)00033-3.

Landis, J. R., & Koch, G. G. (1977). A one-way components of variance model for categorical data. *Biometrics*, *33*(4), 671–679. http://dx.doi.org/10.2307/2529465.

Lefsky, M. A., Cohen, W. B., Parker, G. G., & Harding, D. J. (2002). LiDAR remote sensing for ecosystem studies: LiDAR, an emerging remote sensing technology that directly measures the three-dimensional distribution of plant canopies, can accurately estimate vegetation structural attributes and should be of particular interest to forest, landscape, and global ecologists. *Bioscience*, *52*(1), 19–30. http://dx.doi.org/10.1641/0006-3568(2002)052[0019:LRSFES]2.0.CO;2.

Li, A., Glenn, N. F., Olsoy, P. J., Mitchell, J. J., & Shrestha, R. (2015). Aboveground biomass estimates of sagebrush using terrestrial and airborne LiDAR data in a dryland ecosystem. *Agricultural and Forest Meteorology*, *213*, 138–147. http://dx.doi.org/10.1016/j.agrformet.2015.06.005.

Lieth, H. (1975). Primary production of the major vegetation units of the world. In H. Lieth, & R. H. Whittaker (Eds.), *Primary Productivity of the Biosphere* (pp. 203–215). Berlin Heidelberg: Springer.

Lisein, J., Pierrot-Deseilligny, M., Bonnet, S., & Lejeune, P. (2013). A photogrammetric workflow for the creation of a forest canopy height model from small unmanned aerial system imagery. *Forest*, *4*, 922–944. http://dx.doi.org/10.3390/f4040922.

Liu, Y. Y., Evans, J. P., McCabe, M. F., de Jeu, R. A. M., van Dijk, A. I. J. M., Dolman, A. J., & Saizen, I. (2013a). Changing climate and overgrazing are decimating Mongolian Steppes. *PloS One*, *8*(2), e57599. http://dx.doi.org/10.1371/journal.pone.0057599.

Liu, Y. Y., van Dijk, A. I. J. M., McCabe, M. F., Evans, J. P., & de Jeu, R. A. M. (2013b). Global vegetation biomass change (1988–2008) and attribution to environmental and human drivers. *Global Ecology and Biogeography*, *22*(6), 692–705. http://dx.doi.org/10.1111/geb.12024.

Lowe, D. G. (2004). Distinctive image features from scale-invariant keypoints. *International Journal of Computer Vision*, *60*(2), 91–110.

Ludwig, J. A. (1977). Distributional adaptations of root systems in desert environments. In J. K. Marshall (Ed.), *The belowground ecosystem: A synthesis of plant-associated processes* (pp. 85–90). Fort Collins: Colorado State University.

Ludwig, J. A., Reynolds, J. F., & Whitson, P. D. (1975). Size-biomass relationships of several Chihuahuan desert shrubs. *American Midland Naturalist*, *94*(2), 451–461.

Lufafa, A., Diédhiou, I., Ndiaye, N. A. S., Séné, M., Kizito, F., Dick, R. P., & Noller, J. S. (2009). Allometric relationships and peak-season community biomass stocks of native shrubs in Senegal's Peanut Basin. *Journal of Arid Environments*, *73*(3), 260–266. http://dx.doi.org/10.1016/j.jaridenv.2008.09.020.

Mannetje, L.'t. (2000). Measuring biomass of grassland vegetation. In L.'t. Mannetje, & R. M. Jones (Eds.), *Field and Laboratory Methods for Grassland and Animal Production Research* (pp. 151–178). Ney York, NY, USA: CABI Publishing.

Mata-González, R., Sosebee, R. E., & Wan, C. (2002). Shoot and root biomass of desert grasses as affected by biosolids application. *Journal of Arid Environments*, *50*(3), 477–488. http://dx.doi.org/10.1006/jare.2001.0897.

McNeil, B. E., Pisek, J., Lepisk, H., & Flamenco, E. A. (2016). Measuring leaf angle distribution in broadleaf canopies using UAVs. *Agricultural and Forest Meteorology*, *218–219*, 204–208. http://dx.doi.org/10.1016/j.agrformet.2015.12.058.

Miller, E. L., Meeuwig, R. O., & Budy, J. D. (1981). Biomass of Singleleaf Pinyon and Utah Juniper. *United States Department of Agriculture, Forest Service*. Intermountain Forest and Range Experimental Station.

Miller, P. M., Eddleman, L. E., & Kramer, S. (1990). Allocation patterns of carbon and minerals in juvenile and small-adult *Juniperus occidentalis*. *Forest Science*, *36*(3), 734–747.

Mirik, M., Chaudhuri, S., Surber, B., Ale, S., & Ansley, R. J. (2013). Evaluating biomass of Juniper Trees (*Juniperus pinchotii*) from imagery-derived canopy area using the support vector machine classifier. *Advances in Remote Sensing*, *2*, 181–192. http://dx.doi.org/10.4236/ars.2013.22021.

Mitchell, J. J., Glenn, N. F., Sankey, T. T., Derryberry, D. R., Anderson, M. O., & Hruska, R. C. (2011). Small-footprint LiDAR estimations of sagebrush canopy characteristics. *Photogrammetric Engineering & Remote Sensing*, *77*(5), 521–530. http://dx.doi.org/10.14358/PERS.77.5.521.

Mokany, K., Raison, R. J., & Prokushkin, A. S. (2006). Critical analysis of root: Shoot ratios in terrestrial biomes. *Global Change Biology*, *12*(1), 84–96. http://dx.doi.org/10.1111/j.1365-2486.2005.001043.x.

Moore, D. I. (2015). Core research site web seasonal biomass and seasonal and annual NPP data for the net primary production study at the Sevilleta National Wildlife Refuge, New Mexico (1999–2014). *Albuquerque, NM: Sevilleta long term ecological research site database: SEV182* (http://sev.lternet.edu/data/sev-182).

Muldavin, E. H., Moore, D. I., Collins, S. L., Wetherill, K. R., & Lightfoot, D. C. (2008). Aboveground net primary production dynamics in a northern Chihuahuan Desert ecosystem. *Oecologia*, *155*, 123–132.

Murray-Tortarolo, G., et al. (2016). The carbon cycle in Mexico: Past, present and future of C stocks and fluxes. *Biogeosciences*, *13*(1), 223–238. http://dx.doi.org/10.5194/bg-13-223-2016.

Muukkonen, P., & Heiskanen, J. (2007). Biomass estimation over a large area based on standwise forest inventory data and ASTER and MODIS satellite data: A possibility to verify carbon inventories. *Remote Sensing of Environment*, *107*(4), 617–624. http://dx.doi.org/10.1016/j.rse.2006.10.011.

Nafus, A. M., McClaran, M. P., Archer, S. R., & Throop, H. L. (2009). Multispecies allometric models predict grass biomass in semidesert rangeland. *Rangeland Ecology & Management*, *62*(1), 68–72.

Neufeld, H. S., Meinzer, F. C., Wisdom, C. S., Sharifi, M. R., Rundel, P. W., Neufeld, M. S., ... Cunningham, G. L. (1988). Canopy architecture of *Larrea tridentata* (DC.) Cov., a desert shrub: Foliage orientation and direct beam radiation interception. *Oecologia*, *75*(1), 54–60. http://dx.doi.org/10.1007/BF00378813.

Norris, M. D., Blair, J. M., Johnson, L. C., & McKane, R. B. (2001). Assessing changes in biomass, productivity, and C and N stores following *Juniperus virginiana* forest expansion into tallgrass prairie. *Canadian Journal of Forest Research, 31*, 1940–1946.

Northup, B. K., Zitzer, S. F., Archer, S., McMurtry, C. R., & Boutton, T. W. (2005). Aboveground biomass and carbon and nitrogen content of woody species in a subtropical thornscrub parkland. *Journal of Arid Environments*, *62*(1), 23–43. http://dx.doi.org/10.1016/j.jaridenv.2004.09.019.

Nouwakpo, S. K., Weltz, M. A., & McGwire, K. (2015). Assessing the performance of structure-from-motion photogrammetry and terrestrial LiDAR for reconstructing soil surface microtopography of naturally vegetated plots. *Earth Surface Processes and Landforms*. http://dx.doi.org/10.1002/esp.3787 (n/a–n/a).

Nowak, R. S., Moore, D. J., & Tausch, R. J. (1999). *Ecophysiological patterns of pinyon and juniper.* USDA Forest Service Proceedings.

Owe, M., de Jeu, R., & Walker, J. (2001). A methodology for surface soil moisture and vegetation optical depth retrieval using the microwave polarization difference index. *IEEE Transactions on Geoscience and Remote Sensing*, *39*(8), 1643–1654. http://dx.doi.org/10.1109/36.942542.

Padilla, F. M., Miranda, J. D., Jorquera, M. J., & Pugnaire, F. I. (2009). Variability in amount and frequency of water supply affects roots but not growth of arid shrubs. *Plant Ecology*, *204*(2), 261–270.

Parsons, A. J., Abrahams, A. D., & Luk, S. -H. (1990). Hydraulics of interrill overland flow on a semi-arid hillslope, southern Arizona. *Journal of Hydrology*, *117*, 255–273. http://dx.doi.org/10.1016/0022-1694(90)90096-G.

Peters, D. P. C. (2002). Plant species dominance at a grassland–shrubland ecotone: An individual-based gap dynamics model of herbaceous and woody species. *Ecological Modelling, 152*, 5–32.

Popescu, S. C., Wynne, R. H., & Nelson, R. F. (2003). Measuring individual tree crown diameter with lidar and assessing its influence on estimating forest volume and biomass. *Canadian Journal of Remote Sensing*, *29*(5), 564–577. http://dx.doi.org/10.5589/m03-027.

Poulter, B., et al. (2014). Contribution of semi-arid ecosystems to interannual variability of the global carbon cycle. *Nature*, *509*(7502), 600–603. http://dx.doi.org/10.1038/nature13376.

Pregitzer, K. S., DeForest, J. L., Burton, A. J., Allen, M. F., Ruess, R. W., & Hendrick, R. L. (2002). Fine root architecture of nine North American trees. *Ecological Monographs*, *72*(2), 293–309. http://dx.doi.org/10.1890/0012-9615(2002)072[0293:FRAONN]2.0.CO;2.

Puliti, S., Ørka, H. O., Gobakken, T., & Næsset, E. (2015). Inventory of small forest areas using an unmanned aerial system. *Remote Sensing*, *7*(8), 9632–9654. http://dx.doi.org/10.3390/rs70809632.

Puttock, A. (2013). *Vegetation change and water, sediment and carbon dynamics in semi-arid environments.* University of Exeter.

Puttock, A. K., Cunliffe, A. M., Anderson, K., & Brazier, R. E. (2015). Monitoring the impact of Eurasian beaver reintroduction on ecosystem structure using aerial photography collected from a multi-rotor drone. *Journal of Unmanned Vehicle Systems*, *3*(3), 123–130. http://dx.doi.org/10.1139/juvs-2015-0005.

Puttock, A., Dungait, J. A. J., Macleod, C. J. A., Bol, R., & Brazier, R. E. (2014). Woody plant encroachment accelerates erosion of previously stable organic carbon from dryland soils. *Journal of Geophysical Research – Biogeosciences*. http://dx.doi.org/10.1002/2014JG002635 (2014JG002635).

Puttock, A., Macleod, C. J. A., Bol, R., Dungait, J. A. J., & Brazier, R. E. (2013). Changes in ecosystem structure, function and hydrological connectivity in semi-arid grass to woody vegetation transitions. *Earth Surface Processes and Landforms*, *38*(13), 1602–1611. http://dx.doi.org/10.1002/esp.3455.

Rango, A., Laliberte, A., Herrick, J. E., Winters, C., Havstad, K., Steele, C., & Browning, D. (2009). Unmanned aerial vehicle-based remote sensing for rangeland assessment, monitoring, and management. *Journal of Applied Remote Sensing, 3* (033542–033542–15).

Rango, A., Laliberte, A., Steele, C., Herrick, J. E., Bestelmeyer, B., Schmugge, T., ... Jenkins, V. (2006). Using unmanned aerial vehicles for rangelands: Current applications and future potentials. *Environmental Practice*, *8*(3), 159–168. http://dx.doi.org/10.1017/S1466046606060224.

Remondino, F., Spera, M. G., Nocerino, E., Menna, F., & Nex, F. (2014). State of the art in high density image matching. *The Photogrammetric Record*, *29*(146), 144–166. http://dx.doi.org/10.1111/phor.12063.

Roderick, M. L., Chewings, V. H., & Smith, R. C. G. (2000). Remote sensing in vegetation and animal studies. In L.'t. Mannetje, & R. M. Jones (Eds.), *Field and Laboratory Methods for Grassland and Animal Production Research* (pp. 205–226). Ney York, NY, USA: CABI Publishing.

Rozas, V., DeSoto, L., & Olano, J. M. (2009). Sex-specific, age-dependent sensitivity of tree-ring growth to climate in the dioecious tree *Juniperus thurifera*. *New Phytologist*, *182*(3), 687–697. http://dx.doi.org/10.1111/j.1469-8137.2009.02770.x.

Sankey, T., Shrestha, R., Sankey, J. B., Hardegree, S., & Strand, E. (2013). Lidar-derived estimate and uncertainty of carbon sink in successional phases of woody encroachment. *Journal of Geophysical Research – Biogeosciences*, *118*(3), 1144–1155. http://dx.doi.org/10.1002/jgrg.20088.

Schlesinger, W. H. (1997). *Biogeochemistry: An analysis of global change* (2nd ed.). San Diego, CA, USA: Academic Press.

Schlesinger, W. H., & Bernhardt, E. S. (2013a). Chapter 5 — The biosphere: The carbon cycle of terrestrial ecosystems. In W. H. S. S. Bernhardt (Ed.), *Biogeochemistry (third edition)* (pp. 135–172). Boston: Academic Press.

Schlesinger, W. H., & Bernhardt, E. S. (2013b). Chapter 6 — The biosphere: Biogeochemical cycling on land. In W. H. S. S. Bernhardt (Ed.), *Biogeochemistry (Third Edition)* (pp. 173–231). Boston: Academic Press.

Schlesinger, W. H., & Pilmanis, A. M. (1998). Plant–soil interactions in deserts. *Biogeochemistry*, *42*, 169–187. http://dx.doi.org/10.1023/A:1005939924434.

Schlesinger, W. H., Reynolds, J. F., Cunningham, G. L., Huenneke, L. F., Jarrell, W. M., Virginia, R. A., & Whitford, W. G. (1990). Biological feedbacks in global desertification. *Science*, *247*, 1043–1048. http://dx.doi.org/10.1126/science.247.4946.1043.

Scott, R. L., Biederman, J. A., Hamerlynck, E. P., & Barron-Gafford, G. A. (2016). The carbon balance pivot point of southwestern U.S. semiarid ecosystems: Insights from the 21st century drought. *Journal of Geophysical Research – Biogeosciences*. http://dx.doi.org/10.1002/2015JG003181 (2015JG003181).

Shahbazi, M., Sohn, G., Théau, J., & Menard, P. (2015). Development and evaluation of a UAV-photogrammetry system for precise 3D environmental modeling. *Sensors*, *15*(11), 27493–27524. http://dx.doi.org/10.3390/s151127493.

Sims, P. L., Singh, J. S., & Lauenroth, W. K. (1978). The structure and function of ten Western North American grasslands: I. abiotic and vegetational characteristics. *Journal of Ecology*, *66*, 251–285. http://dx.doi.org/10.2307/2259192.

Singh, S. P. (1964). *Cover, biomass, and root-shoot habit of Larrea divaricata on a selected site in southern New Mexico, MSc.* Las Cruces, New Mexico, USA: New Mexico State University.

Smith, M. W., & Vericat, D. (2015). From experimental plots to experimental landscapes: Topography, erosion and deposition in sub-humid badlands from structure-from-motion photogrammetry. *Earth Surface Processes and Landforms*. http://dx.doi.org/10.1002/esp.3747 (n/a–n/a).

Smith, W. B., & Brand, G. J. (1983). *Allometric biomass equations for 98 species of herbs, shrubs and small trees, research note.* USA: U.S. Dept. of Agriculture, Forest Service, North Central Forest Experiment Station, St. Paul, MN.

Sona, G., Pinto, L., Pagliari, D., Passoni, D., & Gini, R. (2014). Experimental analysis of different software packages for orientation and digital surface modelling from UAV images. *Earth Science Informatics*, *7*(2), 97–107. http://dx.doi.org/10.1007/s12145-013-0142-2.

Stewart, J., Parsons, A. J., Wainwright, J., Okin, G. S., Bestelmeyer, B., Fredrickson, E. L., & Schlesinger, W. H. (2014). Modelling emergent patterns of dynamic desert ecosystems. *Ecological Monographs*, *84*(3), 373–410. http://dx.doi.org/10.1890/12-1253.1.

Strand, E. K., Vierling, L. A., Smith, A. M. S., & Bunting, S. C. (2008). Net changes in aboveground woody carbon stock in western juniper woodlands, 1946–1998. *Journal of Geophysical Research, Biogeosciences*, *113*(G1). http://dx.doi.org/10.1029/2007JG000544.

Taylor, J. R. (1997). *An introduction to error analysis: The study of uncertainties in physical measurements.* Sausalito, CA, USA: University Science Books.

Thomas, S. C., & Martin, A. R. (2012). Carbon content of tree tissues: A synthesis. *Forest*, *3*(2), 332–352. http://dx.doi.org/10.3390/f3020332.

Tonkin, T. N., Midgley, N. G., Graham, D. J., & Labadz, J. C. (2014). The potential of small unmanned aircraft systems and structure-from-motion for topographic surveys: A test of emerging integrated approaches at Cwm Idwal, North Wales. *Geomorphology*, *226*, 35–43. http://dx.doi.org/10.1016/j.geomorph.2014.07.021.

Turnbull, L., Wainwright, J., & Brazier, R. E. (2010b). Changes in hydrology and erosion over a transition from grassland to shrubland. *Hydrological Processes*, *24*, 393–414. http://dx.doi.org/10.1002/hyp.7491.

Turnbull, L., Wainwright, J., Brazier, R. E., & Bol, R. (2010a). Biotic and abiotic changes in ecosystem structure over a shrub-encroachment gradient in the Southwestern USA. *Ecosystems*, *13*, 1239–1255. http://dx.doi.org/10.1007/s10021-010-9384-8.

Turnbull, L., Wainwright, J., & Brazier, R. E. (2008). A conceptual framework for understanding semi-arid land degradation: Ecohydrological interactions across multiple-space and time scales. *Ecohydrology*, *1*, 23–34. http://dx.doi.org/10.1002/eco.4.

Turner, D., Lucieer, A., & Wallace, L. (2014). Direct georeferencing of ultrahigh-resolution UAV imagery. *IEEE Transactions on Geoscience and Remote Sensing*, *52*(5), 2738–2745. http://dx.doi.org/10.1109/TGRS.2013.2265295.

Vierling, K. T., Vierling, L. A., Gould, W. A., Martinuzzi, S., & Clawges, R. M. (2008). Lidar: Shedding new light on habitat characterization and modeling. *Frontiers in Ecology and the Environment*, *6*(2), 90–98. http://dx.doi.org/10.1890/070001.

Vierling, L. A., Xu, Y., Eitel, J. U. H., & Oldow, J. S. (2013). Shrub characterization using terrestrial laser scanning and implications for airborne LiDAR assessment. *Canadian Journal of Remote Sensing*, *38*(6), 709–722. http://dx.doi.org/10.5589/m12-057.

Wainwright, J., Parsons, A. J., & Abrahams, A. D. (1999). Rainfall energy under creosotebush. *Journal of Arid Environments*, *43*, 111–120.

Wainwright, J., Parsons, A. J., & Abrahams, A. D. (2000). Plot-scale studies of vegetation, overland flow and erosion interactions: Case studies from Arizona and New Mexico. *Hydrological Processes*, *14*, 2921–2943.

Wallace, A., Bamberg, S. A., & Cha, J. W. (1974). Quantitative studies of roots of perennial plants in the Mojave Desert. *Ecology*, *55*(5), 1160–1162. http://dx.doi.org/10.2307/1940368.

Wardley, N. W., Milton, E. J., & Hill, C. T. (1987). Remote sensing of structurally complex semi-natural vegetation — an example from heathland. *International Journal of Remote Sensing*. http://dx.doi.org/10.1080/01431168708948613.

Westoby, M. J., Brasington, J., Glasser, N. F., Hambrey, M. J., & Reynolds, J. M. (2012). "Structure-from-motion" photogrammetry: A low-cost, effective tool for geoscience applications. *Geomorphology*, *179*, 300–314. http://dx.doi.org/10.1016/j.geomorph.2012.08.021.

White, M. A., et al. (2009). Intercomparison, interpretation, and assessment of spring phenology in North America estimated from remote sensing for 1982–2006. *Global Change Biology*, *15*(10), 2335–2359. http://dx.doi.org/10.1111/j.1365-2486.2009.01910.x.

Whitford, W. G., Martinez Meza, E., & DeSoyza, A. (1995). In J. R. Barrow, E. Durant, R. E. Sosebee, & R. J. Tausch (Eds.), *Morphological variation in creosotebush, Larrea tridentata: Effects on ecosystem properties, vol. General Technical Report. INT-GTR 338.* (pp. 195–198). U.S.: Department of Agriculture, Forest Service Intermountain Research Station.

Wilson, A. M., Silander, J. A., Gelfand, A., & Glenn, J. H. (2011). Scaling up: Linking field data and remote sensing with a hierarchical model. *International Journal of Geographical Information Science*, *25*(3), 509–521. http://dx.doi.org/10.1080/13658816.2010.522779.

Wilson, B. F. (1995). Shrub stems: Form and functions. In B. L. Gartner (Ed.), *Plant stems: Physiology and functional morphology* (pp. 91–104). San Diego, California, USA: Academic Press.

Woodget, A. S., Carbonneau, P. E., Visser, F., & Maddock, I. P. (2015). Quantifying submerged fluvial topography using hyperspatial resolution UAS imagery and structure from motion photogrammetry. *Earth Surface Processes and Landforms*, *40*(1), 47–64. http://dx.doi.org/10.1002/esp.3613.

Yao, J., Peters, D. P. C., Havstad, K. M., Gibbens, R. P., & Herrick, J. E. (2006). Multi-scale factors and long-term responses of Chihuahuan Desert grasses to drought. *Landscape Ecology*, *21*, 1217–1231. http://dx.doi.org/10.1007/s10980-006-0025-8.

Zahawi, R. A., Dandois, J. P., Holl, K. D., Nadwodny, D., Reid, J. L., & Ellis, E. C. (2015). Using lightweight unmanned aerial vehicles to monitor tropical forest recovery. *Biological Conservation*, *186*, 287–295. http://dx.doi.org/10.1016/j.biocon.2015.03.031.

Zhang, X., & Kondragunta, S. (2006). Estimating forest biomass in the USA using generalized allometric models and MODIS land products. *Geophysical Research Letters*, *33*(9), L09402. http://dx.doi.org/10.1029/2006GL025879.

Zhang, X., Friedl, M. A., Schaaf, C. B., Strahler, A. H., Hodges, J. C. F., Gao, F., ... Huete, A. (2003). Monitoring vegetation phenology using MODIS. *Remote Sensing of Environment*, *84*(3), 471–475. http://dx.doi.org/10.1016/S0034-4257(02)00135-9.